Hepatic accumulation of S-Adenosylmethionine in hamsters with non-alcoholic fatty liver disease associated to metabolic syndrome under selenium and vitamin E deficiency.

Josep Maria del Bas[1,7], Benjamín Rodríguez[2], Francesc Puiggròs[1,7], Silvia Mariné[3], Miguel Angel Rodríguez[3], David Moriña[4,5], Lluís Armengol[2], Antoni Caimari[1,7], Lluís Arola[1,6]

[1] Nutrition and Health Unit. EURECAT-Technology Centre of Catalonia, Reus, Spain.

[2]R&D, Department, Quantitative Genomic Medicine Laboratories (qGenomics), Barcelona, Spain.

[3]Centre for Omic Sciences, Universitat Rovira i Virgili (COS-URV). Reus, Tarragona. Spain.

[4]Centre for Research in Environmental Epidemiology (CREAL), Universitat Pompeu Fabra (UPF), CIBER Epidemiología y Salud Pública (CIBERESP), 08003 Barcelona, Spain

[5]Grups de Recerca d'Àfrica i Amèrica Llatines (GRAAL), Unitat de Bioestadística, Facultat de Medicina, Universitat Autònoma de Barcelona, 08193 Cerdanyola del Vallès, Spain.

[6]Nutrigenomics Research Group, Departament de Bioquímica i Biotecnologia, Universitat Rovira i Virgili, Tarragona, Spain.

[7]Nutrition and Health research group (GRNS). EURECAT-Technology Centre of Catalonia, Reus, Spain.

Corresponding author: Antoni Caimari. CTNS. Avd Universitat, 1. 43204. Reus, Tarragona. Spain. Telf: 0034 977 751 720. Fax: 0034 977 300 431. antoni.caimari@ctns.cat

Abbreviations: AMPK, AMP-activated protein kinase; HCC, hepatocellular carcinoma; Hcy, homocysteine; HFD, high fat diet; HOMA-IR, homeostatic model assessment insulin resistance; IPA, integrated pathway analysis ; MCD, methionine and choline deficient diet; MetS, metabolic syndrome; mHFD, conventional high fat diet; NAFLD, non-alcoholic fatty liver

disease; NASH, non-alcoholic steatohepatitis; NMR, nuclear magnetic resonance; SAH, s-adenosylhomocysteine; SAM, s-adenosylmethionine ; Se, selenium; STD, standard diet

Perspectives

- **Background:** Non-alcoholic fatty liver disease (NAFLD) is considered the hepatic manifestation of metabolic syndrome (MetS), but more research in reliable preclinical models is needed in order to understand the progression of NAFLD in such context.
- **Results:** We developed a preclinical model by challenging golden hamsters with a high fat diet low in selenium and vitamin E. As expected, hamsters presented MetS accompanied by the onset of non-alcoholic steatohepatitis (NASH). Nevertheless, metabolomics and transcriptomics integrated analysis revealed an unexpected hepatic accumulation of S-Adenosylmethionine (SAM) associated to NAFLD progression in our model.
- **Significance of the results to human health and disease**: Our results suggest that progression of NAFLD in the context of MetS can take place even in a situation of hepatic SAM excess and that assessment of selenium and vitamin E status might be considered in current therapies against NASH based on SAM supplementation.

Abstract

Progression of non-alcoholic fatty liver disease (NAFLD) in the context of metabolic syndrome (MetS) is only partially explored due to the lack of preclinical models. In order to study the alterations in hepatic metabolism that accompany this condition, we developed a model of MetS accompanied by the onset of steatohepatitis (NASH) by challenging golden hamsters with a high fat diet low in vitamin E and selenium (HFD), since combined deficiency results in hepatic necroinflammation in rodents. Metabolomics and transcriptomics integrated analyses of livers revealed an unexpected accumulation of hepatic S-Adenosylmethionine (SAM) when compared with healthy livers likely due to diminished methylation reactions and repression of GNMT. SAM plays a key role in the maintenance of cellular homeostasis and cell cycle control. In agreement, analysis of overrepresented transcription factors revealed a central role of c-myc and c-Jun pathways accompanied by negative correlations between SAM concentration, MYC expression and AMPK phosphorylation. These findings point to a drift of cell cycle control towards senescence in livers of HFD animals, which could explain the onset of NASH in this model. In contrast, hamsters with NAFLD induced by a conventional high fat diet did not show SAM accumulation, suggesting a key role of selenium and vitamin E in SAM homeostasis. In conclusion, our results suggest that progression of NAFLD in the context of MetS can take place even in a situation of hepatic SAM excess and that selenium and vitamin E status might be considered in current therapies against NASH based on SAM supplementation.

Introduction

Among the different processes altered during NAFLD progression, impairment of the one carbon metabolism is of special relevance due to its role as a source of precursors for different key cellular processes [1–3]. In this metabolism, the methionine cycle functions as a hub. Thus, methionine can be converted to s-adenosylmethionine (SAM), the main substrate of cellular methylation reactions. SAM has a wide array of fates, such as methylation of proteins and DNA to modulate the stability of the genome or the biosynthesis of several metabolites such as phosphatidylcholine for VLDL synthesis and secretion, polyamines or creatine among others [4–6]. Beyond its role as a methyl donor, it has been suggested that SAM may act as well as a metabolic regulator in the liver, controlling processes such as regeneration, differentiation and the sensitivity of the organ to different insults [4]. Thus, different works have linked the overexpression of the proto-oncogene c-myc to SAM deficiency in cirrhosis and HCC [7–9]. S-adenosylhomocysteine (SAH) is the result of using the methyl group of SAM in methylation reactions. In turn, SAH can be transformed to homocysteine (Hcy), which can enter the transulfuration pathway for the synthesis of antioxidants such as glutathione and taurine or remethylated back to methionine to complete the cycle [5,10].

The relevance of the methionine cycle in the progression of NAFLD has been outlined by several studies in pre-clinical models such as transgenic mice [3] and the methionine and choline deficient diet fed rodent (MCD) [11]. In these models, gene deletion or the deficiency of labile methyl groups in the form of methionine and choline directly disrupts

88 the capacity of synthetizing SAM, a situation that leads to development of steatosis and
89 a rapid progression towards NASH, cirrhosis and HCC [7–9]. Studies in human subjects
90 also support that alterations of the methionine cycle and decreased levels of SAM are
91 associated to advanced stages of NAFLD, such as cirrhosis and HCC [3]. All these
92 evidences points to SAM supplementation as a promising therapy against NASH
93 development and progression [3,5,10,12]. Nevertheless, human studies in initial stages of
94 NASH are not yet possible due to the lack of early diagnosis. Besides, MCD based models
95 do not fully resemble the human condition, since MCD does not result in the main
96 components of the MetS that usually accompany NAFLD, such as dyslipidemia, obesity,
97 adipose tissue dysfunction or insulin resistance[11]. Therefore, the interplay between the
98 systemic dysregulations associated to MetS, the alterations of the methionine cycle and
99 the progression of NAFLD cannot be studied in these models [11,13]. On the other hand,
100 conventional high fat diets are useful to induce fatty liver, but usually fail to induce more
101 advanced stages of NAFLD such as NASH or cirrhosis, which involve hepatocyte death,
102 inflammation or fibrosis among other components [11,13]. In this context, it has been
103 shown that dietary depletion of either Selenium (Se) or vitamin E individually has minor
104 consequences for liver health, but the simultaneous lack of both components results in
105 severe liver damage, causing cell death in both rat and mice (reviewed in [14]).
106 Accordingly, simultaneous but not individual depletion of both components results in a
107 hepatic gene expression profile that suggests inflammation, apoptosis and reduced
108 antioxidant defence in rats [15]. In this sense, the vitamin E and Se deficient diet
109 resembles a MCD diet. Nevertheless, the proposed mechanisms underlying the effects of
110 vitamin E and Se deficiency involves alteration of the antioxidant machinery of cells,
111 leading to exacerbated oxidative damage and subsequent cell death [14], a mechanism
112 that has also been proposed as a trigger for the progression of NAFLD [2,16] and, at first

glance, is closer to the etiology of NAFLD than the MCD diet. Moreover, decreasing levels of plasma Se correlates with progression of NAFLD [17,18] and is associated to MetS in humans [19,20]. Finally, NAFLD in humans has been associated to poor vitamin E consumption and, in accordance, vitamin E therapy has led to positive outcomes [16]. Therefore, we hypothesized that combining the effects of a classical high fat and cholesterol diet with the effects of Se and vitamin E deficiency would result in a reliable model to study the progression of NAFLD towards NASH in the context of MetS.

Our main objective was to study the alterations in the hepatic transcriptome and the components of the metabolome surrounding the one carbon metabolism that are associated to the progression of NAFLD. To do that, we chose the golden Syrian hamster as a model due to the similarities that these animals share with humans but not mice or rats regarding the hepatic metabolism of lipids and lipoproteins [21–24]. Hamsters were fed a high fat and cholesterol diet with low levels of vitamin E and Se. As a result, we obtained a model of MetS accompanied by the onset of NASH. In this model we studied the alterations in hepatic metabolome and transcriptome, together with the transcription factor network that governs the gene expression program, during NAFLD progression. Surprisingly, we found increased levels of SAM in NASH livers, a situation that contrast with previous works, suggesting that NAFLD can progress even under an excess of hepatic SAM.

Materials and Methods

Animals, diets and plasma analyses

The animal protocol was reviewed and approved by the Bioethical Committee of the University Rovira i Virgili and guidelines for the use and care of laboratory animals of the university were followed. All methods were carried out in accordance with the approved guidelines.

Twenty 23 days-old male golden syrian hamsters (*Mesocricetus auratus*) were obtained from Charles Rivers Laboratories (Barcelona, Spain) and housed at 22°C with a period of light/dark of 12 h and with free access to food and water. Hamsters were randomly distributed into two experimental groups (n=10) fed *ad libitum* with a standard diet (STD) or a High fat diet without added Se and vitamin E (HFD) (supplementary table 1). At day 120 animals were sacrificed in fasted conditions. Plasma was obtained and stored at -80ºC. Tissues were rapidly removed, weighted, snap-frozen in liquid nitrogen and stored at -80°C until further analyses. A second cohort of hamsters fed a vitamin E and Se balanced HFD (mHFD) and their STD counterparts have been described previously [24]

Analyses of plasma were carried out using commercial kits as previously described [24] and liver histology as described previously [25]. Further details are provided in supplementary materials and methods.

^{1}H NMR analysis for hepatic metabolite determination

Liver samples were pooled two by two obtaining 5 STD samples and 5 HFD samples. Pools were extracted as described previously [26]. ^{1}H NMR spectra were recorded at 300 K on an Avance III 600 spectrometer (Bruker, Germany). Data analysis has been described previously [26]. Further details are provided in supplementary materials and methods.

Hepatic S-adenosylmethionine and S-adenosylhomocysteine analysis.

158 The method has been previously described [27]. Liver samples were extracted and
159 analysed with a 1290 liquid chromatograph coupled to a 6490 tandem mass spectrometer
160 (Agilent Technologies, Palo Alto, U.S.A.). The chromatographic column was an Aquity
161 UPLC C18 HSS T3 (Waters, Milford, U.S.A.). The precursor to product transitions for
162 the quantification were m/z 298.2 to136 for SAM and m/z 385.2 to136.1 for SAH.
163 Detailed information is provided in supplementary materials and methods.

164 *RNA extraction and real time quantitative PCR*

165 Extraction of RNA from liver tissues, cDNA synthesis and Real time-quantitative-PCR
166 were carried out as described previously [28] using the oligonucleotides described in
167 supplementary table 2.

168 *Hamster microarray hybridization and gene expression analysis.*

169 Specific hamster microarrays were from quantitative Genomics Inc. Custom two-colour
170 expression microarrays targeting hamster transcripts were developed by qGenomics
171 laboratory after transcriptome assembly from RNA-Seq data following procedures
172 published elsewhere's [29–31]. Custom 60-mer microarrays printed with SurePrint
173 technology were used for this study (Agilent Technologies, Palo Alto, USA). Microarrays
174 were applied according manufacturer's conditions and data was analysed using limma
175 software [32]. Results of gene expression analysis have been registered with the number
176 GSE76725 in the gene expression omnibus (GEO, NCBI, NIH, Maryland, USA) and are
177 accessible at the GEO website.

178 *Integrated pathway analysis, Transcription factor binding sites gene set enrichment and*
179 *subsequent network analysis*

For integrated pathway analysis (IPA) differentially changed metabolites and transcripts were analyzed with the Metabolanalyst software [33]. For transcription factor binding sites gene set enrichment, differentially expressed genes were analyzed with the ENCODE ChIP-Seq significance tool [34]. Network was generated with the transcription factors that were commonly changed for both human and mouse by using the plug-in Genemania [35] for Cytoscape 3.0.1 software [36] and analyzed with the plug-in CentiScaPe [37] to quantify the centrality parameters degree and eigenvector. Details are described in supplementary materials and methods.

Analysis of DNMTs, GNMT and MAT1A protein and 5-methylcytosine.

Abundance of DNMT1, DNMT3A, MAT1A and GNMT were assayed with ELISA kits after liver homogeneization and protein determination as recommended by the manufacturer (MyBiosource, California, USA). Global DNA methylation was determined as 5-methylcytosine (5-mC) content in total DNA by ELISA (Epigentek, NY, USA) after DNA extraction (Qiagen, Hilden, Germany).

AMPK analysis

Total and phosphorylated AMPK was quantified as described previously [38].

Statistical analysis

All data, except NMR determinations and microarray results, are expressed as the mean ± SEM. Differences between groups were analyzed using Student's t test. For NMR data, the false discovery rate correction was applied to p-values according to the Benjamini-Hochberg method [39] using the software R [40]. For microarray statistics see supplementary materials and methods.

Results

Hamsters fed the HFD develop metabolic syndrome-like alterations

At the end of the experimental period, HFD intake induced obesity, as indicates the significant 24% increase of the adiposity index (table 1). Adipose tissue accretion in the HFD group resulted in increased levels of plasma leptin accompanied by reduced adiponectin and higher concentrations of plasma fatty acids and glycerol, which suggests increased efflux of fatty acids from the adipose tissue (table 2). Insulin resistance and dyslipidemia resulted in higher insulin resistance index HOMA-IR and atherosclerosis risk index, calculated as the LDL-cholesterol/HDL-cholesterol, ratio in the HFD group (table 2). NAFLD has been suggested as the hepatic manifestation of the MetS. Consistently, the alterations described above were accompanied by enlarged and enlightened livers in the HFD group that were further characterized.

Hamsters fed the HFD present hepatocellular damage, hepatic oxidative damage, inflammation and fibrosis.

Histological examination of livers revealed microvesicular steatosis (figure 1A) and Mason's trichrome staining revealed enlarged perivenular and, occasionally, lobular collagen fibres in the HFD respect the STD group (figure 1A), suggesting the onset of fibrosis.

Immune cells infiltration was observed in lobular (Figure 1B) and perivenular (Figure 1C) areas of HFD but not STD livers. This was unbiasedly confirmed by tissue type profiling using the differentially changed genes of the microarray gene expression analysis. Thus, analysis of all the genes changed in the livers of HFD versus the STD animals clearly matched liver tissue, as expected (supplementary figure 1A), but the same

analysis carried out with only the overexpressed genes matched immune cell types (supplementary figure 1B) likely due to the enrichment of the overexpressed genes set with genes exclusively expressed by immune cells.

Hepatocellular damage in the HFD fed animals was confirmed by increased plasma ALT (figure 1D) and AST (figure 1E, p=0.06). The 36% increase in hepatic TBARS (figure 1F) suggested increased lipid peroxidation due to oxidative stress, a characteristic feature of NAFLD. Moreover, we also found increased expression at the mRNA level of C/EBP-Homologous Protein *DDIT3/CHOP* (figure 1G), which has been suggested as a marker of sustained endoplasmic reticulum stress and integrated stress response that takes place in NASH [41]. These results indicate that livers of HFD animals present an advanced NAFLD, but have not yet evolved to cirrhosis.

Metabolomics and transcriptomics integrated pathway analysis reveals dysregulation of the hepatic methionine cycle in HFD hamsters.

An integrated pathway analysis (IPA) of differentially changed genes and metabolites obtained by microarray transcriptomics (supplementary table 3) and NMR metabolomics (supplementary table 4), respectively, revealed important statistically significant changes in pathways related with lipids, aminoacids and carbohydrates metabolisms in livers of HFD animals (figure 2). Thorough analysis of the significantly changed concepts related with aminoacids, namely arginine and proline (supplementary figure 2), beta-alanine (supplementary figure 3) and glutathione (supplementary figure 4) metabolisms, revealed a common link among them, the spermine and spermidine biosynthesis pathway, which belong to the polyamine pathway. Thus, the HFD repressed the expression of hepatic spermidine synthase (*SRM*, Supplementary table 3), the SAM-dependent polyamine biosynthetic enzyme. Besides, different metabolites that were significantly reduced, such

as methionine, creatine or glutathione (figure 3A) are highly dependent on SAM levels [10,42,43], as well as the biosynthesis of PC from PE by means of the SAM –dependent enzyme PEMT, which is critical for VLDL synthesis and secretion to avoid steatosis [44,45]. In HFD hamsters, the concentration of PC (figure 3A) and the gene expression of *PEMT* (supplementary table 3) were decreased respect the STD group, mimicking the situation of human NASH [45]. These evidences, together with other metabolites that were significantly changed in our experiment and are compiled in figures 3A and 3B, prompted us to further analyse the components of the methionine cycle. As expected, SAM (figure 3C) and SAH (figure 3D) were all changed by the HFD. Surprisingly, SAM was increased, as was the SAM/SAH ratio (figure 4F), which has been proposed as an index of methylation activity [3]. Therefore, the increased ratio suggests a decrease of methylation activity.

Hepatic GNMT and global DNA methylation are dysregulated in HFD hamsters

Increased hepatic SAM concentration prompted us to assess the expression of GNMT, a major controller of SAM levels [46]. Results (figure 4B) show a slight but statistically significant 13% decrease of this protein in the HFD group ($p=0.003$). In turn, MAT1A (Figure 4A) remained unchanged. Assessment of global DNA methylation showed a 25% reduction in 5-mC in HFD animals (figure 4C) but no changes in the protein levels of DNA methyltransferases DNMT1 and DNMT3A (Figures 4D and 4E respectively).

Alterations in the hepatic network of transcription factors in HFD hamsters reveal dysregulation of MYC and JUN expression.

The IPA analysis provides information about enzyme-driven metabolic pathways but not about gene programming control. In order to unbiasedly characterize the changes in the

transcription factor network that accompanies the physiological and molecular events described above, we searched for over-represented transcription factor target sites among the differentially expressed genes from the microarray gene expression data. A total of 149 transcription factors were significantly enriched ($q<0.05$) when the human database was used, and 66 for the mouse database, resulting in 24 common hits that were subsequently analysed by constructing an interactions network (figure 5A). The GO terms significantly associated to the network were relevant to cell cycle control beyond the DNA binding-associated terms expected for a transcription factor network (supplementary table 5). Centrality parameters degree and eigenvector (figure 5B) showed that c-Myc presents the most specific weight in the network, closely followed by c-Jun. Therefore, gene expression of these two regulators was further studied by RT-q-PCR, finding that *MYC* was repressed (figure 5C) and *JUN* induced (figure 5D) in the livers of HFD hamsters respect the STD group. It is well known that the expression of *MYC* is related with the levels of SAM, SAH and the ratio SAM/SAH [7–9]. In our model, the levels of *MYC* expression significantly correlated with the abundancy of SAM (Spearman's rank correlation $\rho= -0.6$, $p=0.012$), SAH ($\rho= 0.68$, $p=0.0016$) and the SAM/SAH ratio ($\rho= -0.8$, $p=0.0005$). No significant correlations were found between the levels of *JUN* expression and the above mentioned parameters, although the expression of this gene is upregulated also in mice and human NASH [13]. Overexpression of *JUN* could be explained by sustained activation of the c-Jun N-terminal kinase (JNK) signalling cascade, which responds to a wide array of stimuli, such as FFA, LPC, ER stress, oxidative stress or inflammation [47–50], all of them present in our model.

A Se and vitamin E balanced HFD decrease hepatic SAM concentration.

In order to assess whether a balanced Se and vitamin E HFD impacts the methionine cycle and the expression of *MYC* and *JUN* in NAFLD, we analysed these parameters in livers of a cohort of hamsters previously characterised, fed a STD diet and a Se and VitE balanced high fat diet for 56 days [24]. Concentrations of SAM (figure 6A) and SAH (figure 6B) tended to decrease, though did not reach a statistical significance ($p=0.056$ and $p=0.051$ respectively. The mHFD did not affect SAM/SAH ratio neither the expression of *MYC*. *JUN* presented a tendency ($p=0.099$) towards overexpression though it did not reach statistical significance.

HFD impairs hepatic AMPK phosphorylation.

It has been previously shown that, among other mechanisms such as modulation of *MYC* expression, SAM can control cell cycle by inhibiting the LKB1-dependent phosphorylation of AMPK [9,51,52]. Analysis of phosphorylated AMPK revealed decreased levels in the livers of HFD animals respect the STD group (figure 7). Further analysis revealed statistically significant correlations between SAM and total AMPK ($\rho= -0.65$, $p=0.004$) and phosphorylated AMPK ($\rho= -0.5$, $p=0.04$).

Discussion

According to a wide array of works, combined but not individual depletion of dietary Se and vitamin E leads to cell death in the liver (reviewed in [14]). More recent transcriptomics-based studies described that combined but not individual deficiency of both nutrients results in a gene expression profile that suggests inflammation, enhanced apoptosis and acute phase response together with diminished antioxidant defence in the liver [15]. Because these events are characteristic of NASH and dietary fats, cholesterol, Se and vitamin E status have been associated with the MetS [19,20], we combined Se and vitamin E deficiency with a high fat and cholesterol diet in order to obtain a model of advanced NAFLD accompanied by MetS. This initial objective was accomplished, but we found an unexpected increase in hepatic SAM levels. Despite we have identified several features of human NAFLD in general and, concretely, NASH in our hamster model, advanced liver disease such as cirrhosis or HCC have been associated with reduced levels of hepatic SAM in humans [5,10], and Kalhan SC *et al.* observed that a lower rate of remethylation of homocysteine and transmethylation of methionine occurs in the livers of NASH patients, suggesting a decrease in SAM synthesis in this condition [53]. In MCD pre-clinical models SAM depletion is thought to be a key factor for rapid progression towards NASH, cirrhosis and HCC [11]. Other models, such as transgenic mice lacking MAT activity, the enzyme driving SAM synthesis from methionine, also show spontaneous induction of NASH and increased susceptibility to liver injury [54]. Therefore, the finding of increased SAM in our model was striking at first glance. Nevertheless, accumulation of SAM in GNMT -/- transgenic mice also results in development of NASH and progression towards HCC [46,55], evidencing that NAFLD progression is not necessarily associated with SAM depletion. In agreement with these

works, we found a reduction of GNMT expression. It has been shown that GNMT knockout results in a 50 fold increase in SAM, highlighting the relevance of this protein as a buffer of SAM homeostasis [56]. Despite our results show a slight reduction of the protein, this might be relevant for contributing, at least in part, to the 50% increased levels of SAM observed in livers of HFD animals. Other important enzymes in SAM metabolism such as methionine synthase or Betaine-homocysteine methyltransferase were not changed at the gene expression level as assessed by the transcriptomics analysis. Together with transgenic models (reviewed in [3]), our results suggest that NAFLD progression can occur even when hepatic levels of SAM are high, pointing out that disease progression might be related, in some physiological situations, with altered SAM homeostasis or utilization regardless its intracellular concentration. Importantly, to our knowledge this is the first time that increased hepatic SAM is observed in NAFLD progression associated to diet-induced MetS.

In the livers of HFD animals, either SAM products, such as SAH, creatine, glutathione and PC, or precursors such as methionine were reduced. Moreover, together with GNMT, the expression of some genes coding for SAM-dependent biosynthetic enzymes, such as *PEMT* or *SRM*, was repressed. Also global methylation of DNA was decreased. This finding is in agreement with this event as a hallmark of NAFLD progression [58]. Nevertheless, these results contrast with the increased levels of SAM, since increased concentration has been associated to DNA hypermethylation [57]. Therefore, altogether, it could be hypothesised that our results point to a state were SAM utilization for biosynthetic or methylation reactions is reduced even at the gene program level. In such a situation, GNMT is expected to act as a buffer to compensate SAM levels by increasing its expression and activity. Nevertheless, our results point to a dysregulation of this

buffering system. This situation could be explained by the emerging role of SAM as a key modulator of hepatic regeneration, differentiation and sensitivity to injury [10,59]. Thus, SAM depletion has been observed in proliferating cells during either liver regeneration or HCC [60,61]. On the contrary, senescence is associated with increased SAM levels [9,61]. For example, SAM treatment is pro-apoptotic in rat hepatoma cells [62] and blocks hepatocyte proliferation [51] and liver regeneration in hepatectomized mice [52]. Therefore, it is plausible to hypothesize that, in our model, intracellular SAM accumulation is contributing to trigger the senescence of malfunctioning hepatocytes. In agreement with this hypothesis, transcription factors c-Jun and c-Myc were the most relevant hubs in the network obtained using transcriptomics data. Previous works have demonstrated clear inverse associations between c-Myc expression and SAM levels [7–9,63], and the correlations among SAM, SAM/SAH and *MYC* expression found in our work agree with these findings. Moreover, repression of this proto-oncogene has been described to be pro-apoptotic in cancer cells [8]. Altogether, the increased levels of SAM, the upregulation of *JUN*, the repression of *MYC* and the impaired phosphorylation of AMPK point to a state of cell senescence. This observation is reinforced by the increased serum markers of hepatocellular damage and the onset of fibrosis detected in livers of the HFD group. These results agree with different works showing that NAFLD is linked to accelerated ageing and that hepatocyte senescence is a predictor of progression in NAFLD [64].

The hypothesis exposed above is in agreement with different works in rats fed Se deficient diets. Thus, it has been shown that dietary Se deficiency leads to increased or unchanged hepatic SAM and SAM/SAH in cultured cells and in rats [65,66]. Also in liver of rats, Se restriction leads to decreased GNMT activity, unchanged SAM or SAM/SAH ratio but

383 DNA hypomethylation [67]. The increase of SAM and SAM/SAH ratio together with
384 global DNA hypomethylation and GNMT repression observed in NASH livers of HFD
385 hamsters resemble the situation described by these works. Our results are consistent with
386 a decreased use of SAM for methylation reactions in general, suggesting that our HFD
387 not only impairs DNA methylation but the different reactions dependent of SAM
388 utilization. Moreover, it has been shown that Se impacts the cell cycle control by inducing
389 c-myc expression, among other targets, promoting proliferation of cultured cells, whilst
390 Se deficiency leads to cell death, an effect that can be reversed by vitamin E [68].
391 Therefore, it is plausible to hypothesize that combined Se and vitamin E deficiency are
392 responsible for the increased SAM and inhibited MYC expression in livers of HFD
393 hamsters, a situation that promotes cell senescence and therefore accelerated development
394 of NASH in hamsters under a high fat and cholesterol diet background. In agreement with
395 this hypothesis, hamsters fed a Se and vitamin E balanced high fat diet (mHFD) developed
396 steatosis with a non-significant tendency of decreased SAM concentration and unchanged
397 *MYC* expression. Therefore, it can be hypothesized that the mechanism proposed herein
398 is responsible, at least partially, of the necroinflammatory effects in the liver ascribed to
399 Se and vitamin E combined deficiency described by the previous works that were taken
400 as a base when designing the diets to obtain our preclinical model [14,15].

401 The link between MetS and NAFLD is well accepted. In fact, some authors have proposed
402 that NAFLD is the hepatic manifestation of MetS [11]. Progression of NAFLD involves
403 NASH, cirrhosis and HCC. The relevance of the methionine cycle in the pathophysiology
404 of NAFLD has postulated SAM therapy as a promising strategy against NASH
405 [3,5,10,12]. Nevertheless, in the view of our results and other works in transgenic mice
406 [46,55], increasing hepatic SAM might not be an efficient strategy in some particular

cases where the cellular machinery involved in maintenance of SAM homeostasis is not properly functioning. In this sense, our results suggest that Se and vitamin E status might affect the liver upstream SAM concentration, triggering the development of NASH by a mechanism that involves impairment of SAM utilization and cell senescence. Since both MetS and NAFLD have been associated to states of Se and vitamin E deficiency [17–20], more research is still needed in human cohorts in order to understand the role of dietary Se and vitamin E in the maintenance of hepatic SAM homeostasis and whether SAM therapy should be accompanied by assessment of Se and vitamin E status in order to ameliorate NASH and the progression of NAFLD under the MetS background. In fact, vitamin E therapy against NAFLD has reported positive outcomes [69]. According to our results and previous works [2,70], the alterations in pathways or metabolisms that lead to the development of NASH might differ among individuals depending on genetic background or environmental factors such as nutrition. Identification of the different alterations that can lead to the onset of NASH and development of new biomarkers that allow studying the inter-individual differences of this pathology would result invaluable in order to understand the disease and to find personalized treatments.

Acknowledgements

We gratefully acknowledge the aid of Vanessa Grifoll and Silvia Pijuan, the laboratory technicians, and Sirle Laos, Leonor Conde, Gerard Aragonés, Víctor Cerdán and Anabel Sáez for their advice and technical support.

Declaration of interests: The authors declare no conflict of interests.

Financial support: This study has been supported by CDTI, Convocatoria Industria de la Ciencia IDC-20101073.

Authors contributions

JMdB contributed to study concept and design; acquisition of data; analysis and interpretation of data; drafting of the manuscript; critical revision of the manuscript; statistical analysis and supervised the study.

BR contributed to study concept and design; acquisition of data; analysis and interpretation of data; drafting of the manuscript; critical revision of the manuscript and statistical analysis.

FP contributed to study concept and design; critical revision of the manuscript and funding support.

SM contributed to analysis and interpretation of data; drafting of the manuscript; critical revision of the manuscript and statistical analysis.

MAR contributed to analysis and interpretation of data; drafting of the manuscript; critical revision of the manuscript and statistical analysis.

DM contributed to analysis and interpretation of data; drafting of the manuscript and statistical analysis.

LM contributed to study concept and design; critical revision of the manuscript and funding support.

TC contributed to study concept and design; acquisition of data; analysis and interpretation of data; drafting of the manuscript and critical revision of the manuscript.

LA contributed to study concept and design; critical revision of the manuscript and funding support and supervised the study.

References

[1] Lee TD, Sadda MR, Mendler MH, Bottiglieri T, Kanel G, Mato JM, et al. Abnormal hepatic methionine and glutathione metabolism in patients with alcoholic hepatitis. Alcohol Clin Exp Res 2004;28:173–81. doi:10.1097/01.ALC.0000108654.77178.03.

[2] Veena J, Muragundla A, Sidgiddi S, Subramaniam S. Non-alcoholic fatty liver disease: need for a balanced nutritional source. Br J Nutr 2014:1–15. doi:10.1017/S0007114514002591.

[3] Mato JM, Martínez-Chantar ML, Lu SC. Methionine metabolism and liver disease. Annu Rev Nutr 2008;28:273–93. doi:10.1146/annurev.nutr.28.061807.155438.

[4] Anstee QM, Day CP. S-adenosylmethionine (SAMe) therapy in liver disease: a review of current evidence and clinical utility. J Hepatol 2012;57:1097–109. doi:10.1016/j.jhep.2012.04.041.

[5] Mato JM, Lu SC. Role of S-adenosyl-L-methionine in liver health and injury. Hepatology 2007;45:1306–12. doi:10.1002/hep.21650.

[6] Obeid R, Herrmann W. Homocysteine and lipids: S-adenosyl methionine as a key intermediate. FEBS Lett 2009;583:1215–25. doi:10.1016/j.febslet.2009.03.038.

[7] Lu SC, Huang ZZ, Yang H, Mato JM, Avila MA, Tsukamoto H. Changes in methionine adenosyltransferase and S-adenosylmethionine homeostasis in alcoholic rat liver. Am J Physiol Gastrointest Liver Physiol 2000;279:G178-85.

[8] Luo J, Li Y-N, Wang F, Zhang W-M, Geng X. S-adenosylmethionine inhibits the growth of cancer cells by reversing the hypomethylation status of c-myc and H-ras in human gastric cancer and colon cancer. Int J Biol Sci 2010;6:784–95.

[9] Frau M, Feo F, Pascale RM. Pleiotropic effects of methionine adenosyltransferases deregulation as determinants of liver cancer progression and prognosis. J Hepatol 2013;59:830–41. doi:10.1016/j.jhep.2013.04.031.

[10] Anstee QM, Day CP. S-adenosylmethionine (SAMe) therapy in liver disease: a review of current evidence and clinical utility. J Hepatol 2012;57:1097–109. doi:10.1016/j.jhep.2012.04.041.

[11] Imajo K, Yoneda M, Kessoku T, Ogawa Y, Maeda S, Sumida Y, et al. Rodent models of nonalcoholic fatty liver disease/nonalcoholic steatohepatitis. Int J Mol Sci 2013;14:21833–57. doi:10.3390/ijms141121833.

[12] Purohit V, Abdelmalek MF, Barve S, Benevenga NJ, Halsted CH, Kaplowitz N, et al. Role of S-adenosylmethionine, folate, and betaine in the treatment of alcoholic liver disease: summary of a symposium. Am J Clin Nutr 2007;86:14–24.

[13] Dorn C, Engelmann JC, Saugspier M, Koch A, Hartmann A, Müller M, et al. Increased expression of c-Jun in nonalcoholic fatty liver disease. Lab Investig 2014;94:394–408. doi:10.1038/labinvest.2014.3.

[14] National Research Council (US) Subcommittee on Selenium. Selenium in

494 Nutrition: Revised Edition. Revised Ed. National Academies Press (US); 1983.

495 [15] Fischer A, Pallauf J, Gohil K, Weber SU, Packer L, Rimbach G. Effect of
496 selenium and vitamin E deficiency on differential gene expression in rat liver.
497 Biochem Biophys Res Commun 2001;285:470–5. doi:10.1006/bbrc.2001.5171.

498 [16] Al-Busafi S a, Bhat M, Wong P, Ghali P, Deschenes M. Antioxidant therapy in
499 nonalcoholic steatohepatitis. Hepat Res Treat 2012;2012:947575.
500 doi:10.1155/2012/947575.

501 [17] Rohr-Udilova N, Sieghart W, Eferl R, Stoiber D, Björkhem-Bergman L, Eriksson
502 LC, et al. Antagonistic effects of selenium and lipid peroxides on growth control
503 in early hepatocellular carcinoma. Hepatology 2012;55:1112–21.
504 doi:10.1002/hep.24808.

505 [18] Bettinger D, Schultheiss M, Hennecke N, Panther E, Knüppel E, Blum HE, et al.
506 Selenium levels in patients with hepatitis C virus-related chronic hepatitis, liver
507 cirrhosis, and hepatocellular carcinoma: a pilot study. Hepatology 2013;57:2543–
508 4. doi:10.1002/hep.26142.

509 [19] Wei J, Zeng C, Gong Q, Li X, Lei G, Yang T. Associations between Dietary
510 Antioxidant Intake and Metabolic Syndrome. PLoS One 2015;10:e0130876.
511 doi:10.1371/journal.pone.0130876.

512 [20] Zulet MA, Puchau B, Hermsdorff HHM, Navarro C, Martínez JA. Dietary
513 selenium intake is negatively associated with serum sialic acid and metabolic
514 syndrome features in healthy young adults. Nutr Res 2009;29:41–8.
515 doi:10.1016/j.nutres.2008.11.003.

516 [21] Zhang Z, Wang H, Jiao R, Peng C, Wong YM, Yeung VSY, et al. Choosing
517 hamsters but not rats as a model for studying plasma cholesterol-lowering
518 activity of functional foods. Mol Nutr Food Res 2009;53:921–30.
519 doi:10.1002/mnfr.200800517.

520 [22] Dillard A, Matthan NR, Lichtenstein AH. Use of hamster as a model to study
521 diet-induced atherosclerosis. Nutr Metab (Lond) 2010;7:89. doi:10.1186/1743-
522 7075-7-89.

523 [23] Bravo E, Cantafora A, Calcabrini A, Ortu G. Why prefer the golden Syrian
524 hamster (Mesocricetus auratus) to the Wistar rat in experimental studies on
525 plasma lipoprotein metabolism? Comp Biochem Physiol Part B Biochem Mol
526 Biol 1994;107:347–55. doi:10.1016/0305-0491(94)90058-2.

527 [24] Laos S, Caimari A, Crescenti A, Lakkis J, Puiggròs F, Arola L, et al. Long-term
528 intake of soyabean phytosterols lowers serum TAG and NEFA concentrations,
529 increases bile acid synthesis and protects against fatty liver development in
530 dyslipidaemic hamsters. Br J Nutr 2014;112:663–73.
531 doi:10.1017/S0007114514001342.

532 [25] Del Bas JM, Caimari A, Ceresi E, Arola-Arnal A, Palou A, Arola L, et al.
533 Differential effects of habitual chow-based and semi-purified diets on lipid
534 metabolism in lactating rats and their offspring. Br J Nutr 2015:1–12.
535 doi:10.1017/S0007114514004358.

536 [26] Vinaixa M, Rodríguez MA, Rull A, Beltrán R, Bladé C, Brezmes J, et al.

Metabolomic assessment of the effect of dietary cholesterol in the progressive development of fatty liver disease. J Proteome Res 2010;9:2527–38. doi:10.1021/pr901203w.

[27] van Liempd S, Cabrera D, Mato JM, Falcon-Perez JM. A fast method for the quantitation of key metabolites of the methionine pathway in liver tissue by high-resolution mass spectrometry and hydrophilic interaction ultra-performance liquid chromatography. Anal Bioanal Chem 2013;405:5301–10. doi:10.1007/s00216-013-6883-4.

[28] Caimari A, del Bas JM, Crescenti A, Arola L. Low doses of grape seed procyanidins reduce adiposity and improve the plasma lipid profile in hamsters. Int J Obes 2012;37:576–83.

[29] Grabherr MG, Haas BJ, Yassour M, Levin JZ, Thompson DA, Amit I, et al. Full-length transcriptome assembly from RNA-Seq data without a reference genome. Nat Biotechnol 2011;29:644–52. doi:10.1038/nbt.1883.

[30] Zerbino DR. Using the Velvet de novo assembler for short-read sequencing technologies. Curr Protoc Bioinformatics 2010;Chapter 11:Unit 11.5. doi:10.1002/0471250953.bi1105s31.

[31] Zerbino DR, Birney E. Velvet: algorithms for de novo short read assembly using de Bruijn graphs. Genome Res 2008;18:821–9. doi:10.1101/gr.074492.107.

[32] Ritchie ME, Phipson B, Wu D, Hu Y, Law CW, Shi W, et al. limma powers differential expression analyses for RNA-sequencing and microarray studies. Nucleic Acids Res 2015;43:e47. doi:10.1093/nar/gkv007.

[33] Xia J, Wishart DS. Web-based inference of biological patterns, functions and pathways from metabolomic data using MetaboAnalyst. Nat Protoc 2011;6:743–60. doi:10.1038/nprot.2011.319.

[34] Auerbach RK, Chen B, Butte AJ. Relating genes to function: identifying enriched transcription factors using the ENCODE ChIP-Seq significance tool. Bioinformatics 2013;29:1922–4. doi:10.1093/bioinformatics/btt316.

[35] Warde-Farley D, Donaldson SL, Comes O, Zuberi K, Badrawi R, Chao P, et al. The GeneMANIA prediction server: biological network integration for gene prioritization and predicting gene function. Nucleic Acids Res 2010;38:W214-20. doi:10.1093/nar/gkq537.

[36] Shannon P, Markiel A, Ozier O, Baliga NS, Wang JT, Ramage D, et al. Cytoscape: a software environment for integrated models of biomolecular interaction networks. Genome Res 2003;13:2498–504. doi:10.1101/gr.1239303.

[37] Scardoni G, Petterlini M, Laudanna C. Analyzing biological network parameters with CentiScaPe. Bioinformatics 2009;25:2857–9. doi:10.1093/bioinformatics/btp517.

[38] Crescenti A, del Bas JM, Arola-Arnal A, Oms-Oliu G, Arola L, Caimari A. Grape seed procyanidins administered at physiological doses to rats during pregnancy and lactation promote lipid oxidation and up-regulate AMPK in the muscle of male offspring in adulthood. J Nutr Biochem 2015;In press.

[39] Benjamini Y, Hochberg Y. Controlling the False Discovery Rate: A Practical and Powerful Approach to Multiple Testing. J R Stat Soc Ser B 1995;57:289–300.

[40] R Development Core Team R. R: A Language and Environment for Statistical Computing. R Found Stat Comput 2011;1:409. doi:10.1007/978-3-540-74686-7.

[41] Soon RK, Yan JS, Grenert JP, Maher JJ. Stress signaling in the methionine-choline-deficient model of murine fatty liver disease. Gastroenterology 2010;139:1730–9, 1739.e1. doi:10.1053/j.gastro.2010.07.046.

[42] Zeisel SH. Metabolic crosstalk between choline/1-carbon metabolism and energy homeostasis. Clin Chem Lab Med 2013;51:467–75. doi:10.1515/cclm-2012-0518.

[43] Lu SC, Mato JM. S-adenosylmethionine in liver health, injury, and cancer. Physiol Rev 2012;92:1515–42. doi:10.1152/physrev.00047.2011.

[44] Noga AA, Zhao Y, Vance DE. An unexpected requirement for phosphatidylethanolamine N-methyltransferase in the secretion of very low density lipoproteins. J Biol Chem 2002;277:42358–65. doi:10.1074/jbc.M204542200.

[45] Wattacheril J, Seeley EH, Angel P, Chen H, Bowen BP, Lanciault C, et al. Differential intrahepatic phospholipid zonation in simple steatosis and nonalcoholic steatohepatitis. PLoS One 2013;8:e57165. doi:10.1371/journal.pone.0057165.

[46] Martínez-Chantar ML, Vázquez-Chantada M, Ariz U, Martínez N, Varela M, Luka Z, et al. Loss of the glycine N-methyltransferase gene leads to steatosis and hepatocellular carcinoma in mice. Hepatology 2008;47:1191–9. doi:10.1002/hep.22159.

[47] Kodama Y, Brenner D a. c-Jun N-terminal kinase signaling in the pathogenesis of nonalcoholic fatty liver disease: Multiple roles in multiple steps. Hepatology 2009;49:6–8. doi:10.1002/hep.22710.

[48] Sakurai T, Maeda S, Chang L, Karin M. Loss of hepatic NF-kappa B activity enhances chemical hepatocarcinogenesis through sustained c-Jun N-terminal kinase 1 activation. Proc Natl Acad Sci U S A 2006;103:10544–51. doi:10.1073/pnas.0603499103.

[49] Kamata H, Honda S-I, Maeda S, Chang L, Hirata H, Karin M. Reactive oxygen species promote TNFalpha-induced death and sustained JNK activation by inhibiting MAP kinase phosphatases. Cell 2005;120:649–61. doi:10.1016/j.cell.2004.12.041.

[50] Malhi H, Bronk SF, Werneburg NW, Gores GJ. Free fatty acids induce JNK-dependent hepatocyte lipoapoptosis. J Biol Chem 2006;281:12093–101. doi:10.1074/jbc.M510660200.

[51] Martínez-Chantar ML, Vázquez-Chantada M, Garnacho M, Latasa MU, Varela-Rey M, Dotor J, et al. S-adenosylmethionine regulates cytoplasmic HuR via AMP-activated kinase. Gastroenterology 2006;131:223–32. doi:10.1053/j.gastro.2006.04.019.

[52] Vázquez-Chantada M, Ariz U, Varela-Rey M, Embade N, Martínez-Lopez N, Fernández-Ramos D, et al. Evidence for LKB1/AMP-activated protein kinase/ endothelial nitric oxide synthase cascade regulated by hepatocyte growth factor, S-adenosylmethionine, and nitric oxide in hepatocyte proliferation. Hepatology 2009;49:608–17. doi:10.1002/hep.22660.

[53] Kalhan SC, Edmison J, Marczewski S, Dasarathy S, Gruca LL, Bennett C, et al. Methionine and protein metabolism in non-alcoholic steatohepatitis: evidence for lower rate of transmethylation of methionine. Clin Sci (Lond) 2011;121:179–89. doi:10.1042/CS20110060.

[54] Lu SC, Alvarez L, Huang ZZ, Chen L, An W, Corrales FJ, et al. Methionine adenosyltransferase 1A knockout mice are predisposed to liver injury and exhibit increased expression of genes involved in proliferation. Proc Natl Acad Sci U S A 2001;98:5560–5. doi:10.1073/pnas.091016398.

[55] Varela-Rey M, Martínez-López N, Fernández-Ramos D, Embade N, Calvisi DF, Woodhoo A, et al. Fatty liver and fibrosis in glycine N-methyltransferase knockout mice is prevented by nicotinamide. Hepatology 2010;52:105–14. doi:10.1002/hep.23639.

[56] Varela-Rey M, Fernández-Ramos D, Martínez-López N, Embade N, Gómez-Santos L, Beraza N, et al. Impaired liver regeneration in mice lacking glycine N-methyltransferase. Hepatology 2009;50:443–52. doi:10.1002/hep.23033.

[57] Varela-Rey M, Iruarrizaga-Lejarreta M, Lozano JJ, Aransay AM, Fernandez AF, Lavin JL, et al. S-adenosylmethionine levels regulate the schwann cell DNA methylome. Neuron 2014;81:1024–39. doi:10.1016/j.neuron.2014.01.037.

[58] Brunt EM, Wong VW-S, Nobili V, Day CP, Sookoian S, Maher JJ, et al. Nonalcoholic fatty liver disease. Nat Rev Dis Prim 2015;1:15080. doi:10.1038/nrdp.2015.80.

[59] García-Trevijano ER, Latasa MU, Carretero M V, Berasain C, Mato JM, Avila MA. S-adenosylmethionine regulates MAT1A and MAT2A gene expression in cultured rat hepatocytes: a new role for S-adenosylmethionine in the maintenance of the differentiated status of the liver. FASEB J 2000;14:2511–8. doi:10.1096/fj.00-0121com.

[60] Latasa MU, Boukaba A, García-Trevijano ER, Torres L, Rodríguez JL, Caballería J, et al. Hepatocyte growth factor induces MAT2A expression and histone acetylation in rat hepatocytes: role in liver regeneration. FASEB J 2001;15:1248–50.

[61] Cai J, Mao Z, Hwang JJ, Lu SC. Differential expression of methionine adenosyltransferase genes influences the rate of growth of human hepatocellular carcinoma cells. Cancer Res 1998;58:1444–50.

[62] Ansorena E, García-Trevijano ER, Martínez-Chantar ML, Huang Z-Z, Chen L, Mato JM, et al. S-adenosylmethionine and methylthioadenosine are antiapoptotic in cultured rat hepatocytes but proapoptotic in human hepatoma cells. Hepatology 2002;35:274–80. doi:10.1053/jhep.2002.30419.

[63] Fernandez-Sanchez ME, Gonatopoulos-Pournatzis T, Preston G, Lawlor MA,

664 Cowling VH. S-adenosyl homocysteine hydrolase is required for Myc-induced
665 mRNA cap methylation, protein synthesis, and cell proliferation. Mol Cell Biol
666 2009;29:6182–91. doi:10.1128/MCB.00973-09.

667 [64] Aravinthan A, Scarpini C, Tachtatzis P, Verma S, Penrhyn-Lowe S, Harvey R, et
668 al. Hepatocyte senescence predicts progression in non-alcohol-related fatty liver
669 disease. J Hepatol 2013;58:549–56. doi:10.1016/j.jhep.2012.10.031.

670 [65] Davis CD, Uthus EO. Dietary folate and selenium affect dimethylhydrazine-
671 induced aberrant crypt formation, global DNA methylation and one-carbon
672 metabolism in rats. J Nutr 2003;133:2907–14.

673 [66] Davis CD, Uthus EO, Finley JW. Dietary Selenium and Arsenic Affect DNA
674 Methylation In Vitro in Caco-2 Cells and In Vivo in Rat Liver and Colon. J Nutr
675 2000;130:2903–9.

676 [67] Uthus EO, Ross SA, Davis CD. Differential Effects of Dietary Selenium (Se) and
677 Folate on Methyl Metabolism in Liver and Colon of Rats. Biol Trace Elem Res
678 2006;109:201–14. doi:10.1385/BTER:109:3:201.

679 [68] Huawei Z. Selenium as an essential micronutrient: Roles in cell cycle and
680 apoptosis. Molecules 2009;14:1263–78. doi:10.3390/molecules14031263.

681 [69] Noureddin M, Mato JM, Lu SC. Nonalcoholic fatty liver disease: update on
682 pathogenesis, diagnosis, treatment and the role of S-adenosylmethionine. Exp
683 Biol Med 2015;240:809–20. doi:10.1177/1535370215579161.

684 [70] Lim JW, Dillon J, Miller M. Proteomic and genomic studies of non-alcoholic
685 fatty liver disease--clues in the pathogenesis. World J Gastroenterol
686 2014;20:8325–40. doi:10.3748/wjg.v20.i26.8325.

687

688

689

690 **Table 1: Plasma concentrations of metabolites in hamsters fed with a standard diet**

691 **(STD) or a high fat diet (HFD)**

	STD	HFD
Glucose (mmol/L)	5.0± 0.3	7.1 ± 0.4 *
Insulin (ng/mL)	1.6 ± 0.4	3.3 ± 0.6 *
HOMA-IR	9 ± 2	24± 4 *
Leptin (ng/mL)	0.11 ± 0.03	0.35 ± 0.09 *
Adiponectin (µg/mL)	20.6 ± 0.9	14.2 ± 0.9 *
NEFAs (mmol/L)	0.50 ± 0.05	0.81 ± 0.06 *
Glycerol (mmol/L)	0.34 ± 0.02	0.59 ± 0.05 *
Triglycerides (mmol/dL)	1.25 ± 0.07	2.19 ± 0.17 *
Phospholipids (mmol/L)	2.2 ± 0.1	3.5 ± 0.2 *
Total cholesterol (mmol/L)	3.9 ± 0.3	7.9 ± 0.2 *
LDL-cholesterol (mmol/L)	1.6 ± 0.2	4.5 ± 0.1 *
HDL-cholesterol (mmol/L)	2.3 ± 0.2	3.4 ± 0.2 *
LDLc/HDLc	0.71 ± 0.05	1.36 ± 0.10 *

692

693 Mean ± SEM is represented. * Denotes statistically significant differences versus the

694 STD group (Student's *t* test, $p<0.05$).

695

Table 2: Daily intake, body weight, liver weight, adipose tissue weights and adiposity index and in hamsters fed with a standard diet (STD) or a high fat diet (HFD)

	STD	HFD
Food intake (g/day)	8.7±0.04	8.4±0.03
Energy intake (KJ/day)	142±1	148± 1
Selenium intake (µg/day)	2.00±0.04	0.588±0.05 *
Vitamin E intake (IU/day)	0.478±0.008	0.042±0.007 *
Initial body weight (g)	69±2	70±1
Final body weight (g)	147±4	169±3 *
Liver (g)	4.2 ± 0.2	9.3± 0.3 *
RWAT (g)	1.7 ± 0.1	2.3 ± 0.1 *
MWAT (g)	2.4 ± 0.2	3.1 ± 0.2 *
EWAT (g)	2.3 ± 0.2	3.5 ± 0.2 *
IWAT (g)	4.9 ± 0.4	7.0 ± 0.5 *
Adiposity index (%)	7.8 ± 0.4	9.7 ± 0.5 *
IBAT (g)	0.61 ± 0.05	0.68 ± 0.03

Mean ± SEM is represented. * Denotes statistically significant differences versus the STD group (Student's *t* test, $p<0.05$).

Figure 1. Histology of livers in STD and HFD fed animals. (a). Liver sections of golden hamsters fed a standard diet (STD) or a high fat diet (HFD) during 90 days stained with haematoxylin and Eosin (H&E), Mason's trichrome staining (trichrome) and oil red O staining (ORO), scale bar 50 µm. H&E stained sections revealed immune cell infiltration (b and c), scale bar 50 µm. Plasma alanine aminotransferase (d) and aspartate aminotransferase (e), liver Thiobarbituric reactive species (f) and hepatic expression of DDIT3/CHOP (g) are reported. The mean ± SEM is represented. * $p<0.05$.

Figure 2. Metabolomics and transcriptomics integrated pathway analysis of HFD versus STD groups. The ten most relevant concepts in terms of feature set enrichment p-value are represented. Each concept is accompanied by the KEGG code of the corresponding map between brackets, a graphical representation of the Z-score associated to the feature set enrichment analysis (closed bars) and the Z-score associated to the network degree value (open bars), the number of features matching the concept and an * if the p-value of the feature set enrichment analysis is under 0.05.

Figure 3. HFD alters hepatic metabolites related with the methionine cycle. The fold-change logarithm of the HFD versus the STD comparison is shown for selected metabolites related with the methionine cycle (a). Metabolites were mapped to a methionine cycle and related processes scheme (b) showing the change observed for each metabolite. Closed line arrows denote direct processes and dashed lines denote processes composed by different steps. The levels of SAM (c), SAH (d), and the SAM/SAH ratio (e) are reported as the mean ± SEM. * $p<0.05$; ** $q<0.05$.

Figure 4. HFD reduces GNMT expression and DNA global methylation. Expression levels of MAT1A (a) and GNMT (b) were assessed at the protein level. In parallel, effects on DNA global methylation (c) and protein levels of DNMT1 (d) and DNMT3A (e) were determined. The mean ± SEM is reported. * $p<0.05$

Figure 5. Alterations in the hepatic network of transcription factors and MYC and JUN expression in HFD hamsters. Differentially expressed genes of the HFD/STD comparison were analysed for over-represented transcription factor target genes. Results were subjected to network analysis (a). Black nodes represent identified transcription factors and grey nodes the ten genes mostly related to the network. Edges represent physical interactions (red), common pathways (blue) and gene-gene interactions (black). Centrality parameters Degree and Eigenvector were calculated within the network to reveal the most influent nodes (b). Gene expression of MYC (c) and JUN (d) is reported as the mean ± SEM (n=10). * $p<0.05$.

Figure 6. Hepatic SAM and SAH concentrations and MYC expression are not altered in simple steatosis. Concentration of SAM (a), SAH (b), and the SAM/SAH ratio (c) together with gene expression at the mRNA level of MYC (d) and JUN (e) were quantified in livers of hamsters fed the STD diet or a vitamin E and selenium balanced high fat diet (mHFD). Results are reported as the mean ± SEM (n=10).

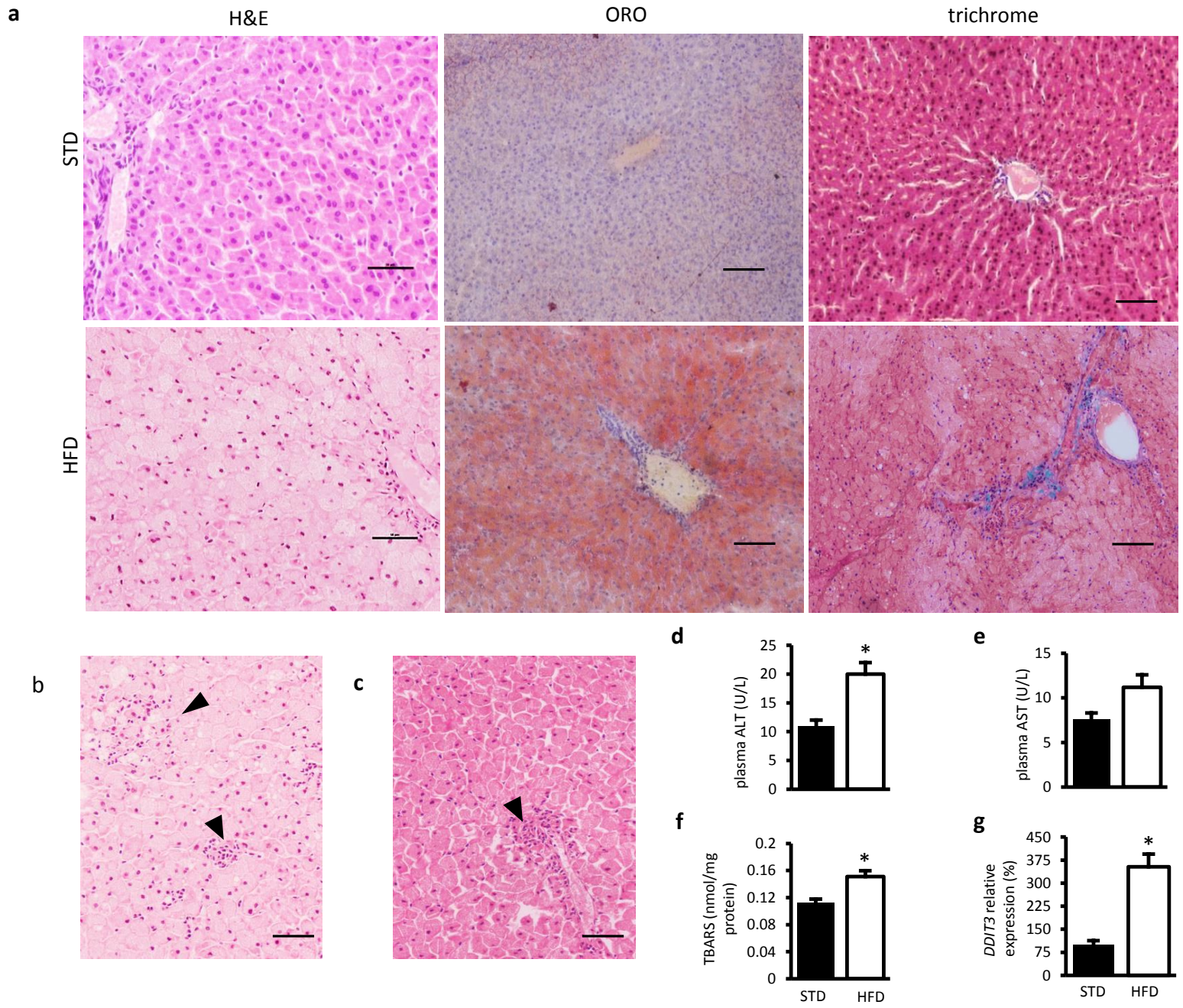
a
H&E
ORO
trichrome
STD
HFD
b
c
d
plasma ALT (U/L)
25
20
15
10
5
0
*
e
plasma AST (U/L)
15
10
5
0
f
TBARS (nmol/mg protein)
0.2
0.16
0.12
0.08
0.04
0
*
STD
HFD
g
DDIT3 relative expression (%)
450
375
300
225
150
75
0
*
STD
HFD

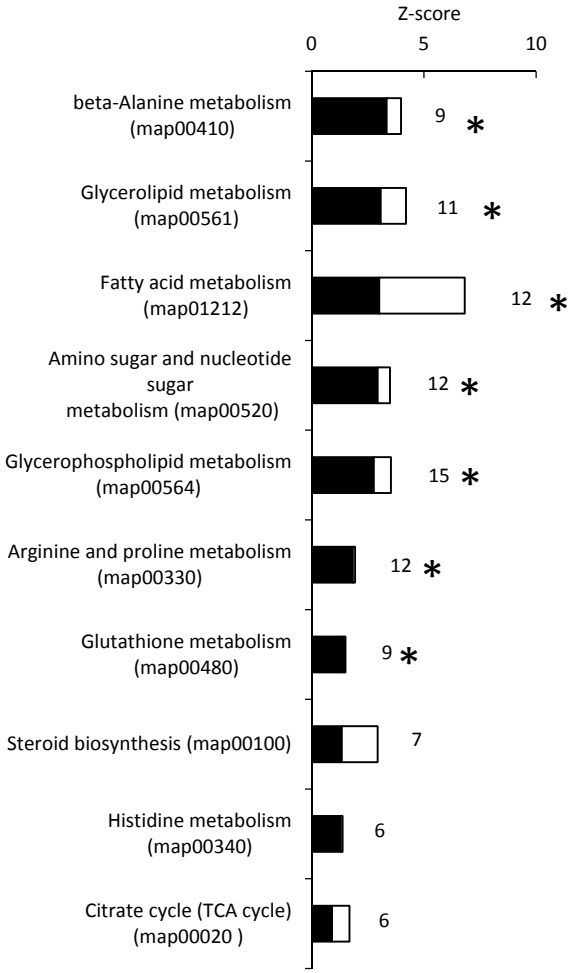
Z-score
0
5
10
beta-Alanine metabolism (map00410)
9
*
Glycerolipid metabolism (map00561)
11
*
Fatty acid metabolism (map01212)
12
*
Amino sugar and nucleotide sugar metabolism (map00520)
12
*
Glycerophospholipid metabolism (map00564)
15
*
Arginine and proline metabolism (map00330)
12
*
Glutathione metabolism (map00480)
9
*
Steroid biosynthesis (map00100)
7
Histidine metabolism (map00340)
6
Citrate cycle (TCA cycle) (map00020)
6

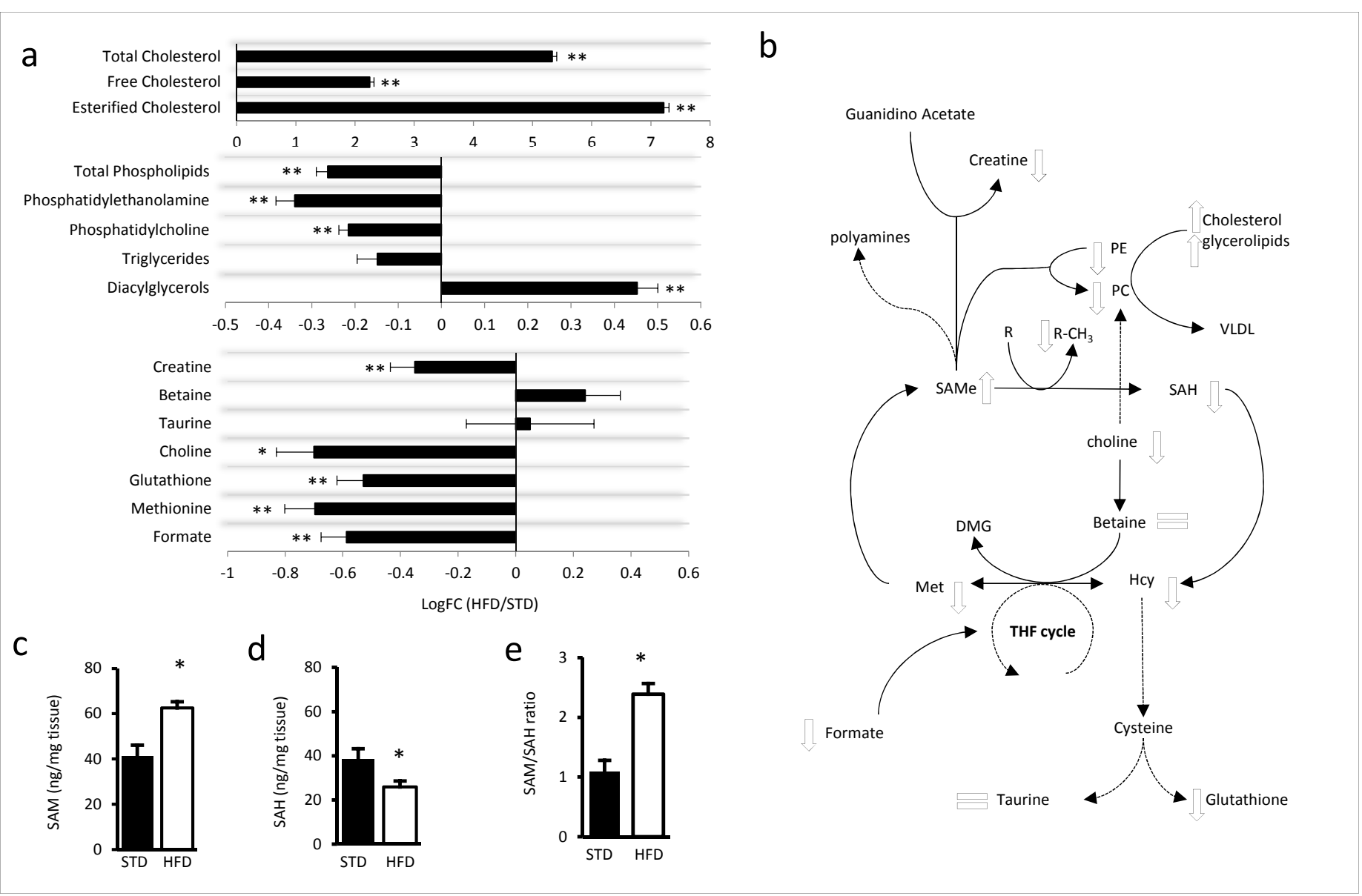
a
Total Cholesterol
Free Cholesterol
Esterified Cholesterol
Total Phospholipids
Phosphatidylethanolamine
Phosphatidylcholine
Triglycerides
Diacylglycerols
Creatine
Betaine
Taurine
Choline
Glutathione
Methionine
Formate
LogFC (HFD/STD)
b
Guanidino Acetate
Creatine
polyamines
PE
PC
Cholesterol
glycerolipids
VLDL
R
R-CH3
SAMe
SAH
choline
DMG
Betaine
Met
Hcy
THF cycle
Formate
Cysteine
Taurine
Glutathione
c
SAM (ng/mg tissue)
STD
HFD
d
SAH (ng/mg tissue)
STD
HFD
e
SAM/SAH ratio
STD
HFD

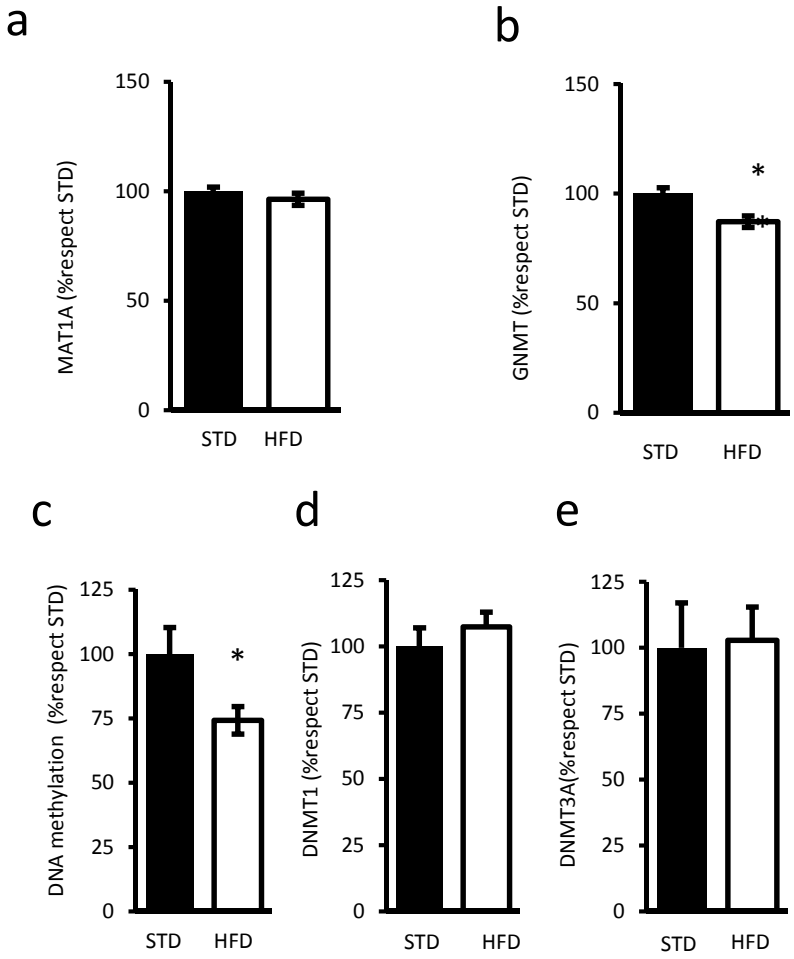
a
MAT1A (%respect STD)
150
100
50
0
STD
HFD
b
GNMT (%respect STD)
150
100
50
0
*
STD
HFD
c
DNA methylation (%respect STD)
125
100
75
50
25
0
*
STD
HFD
d
DNMT1 (%respect STD)
125
100
75
50
25
0
STD
HFD
e
DNMT3A(%respect STD)
125
100
75
50
25
0
STD
HFD

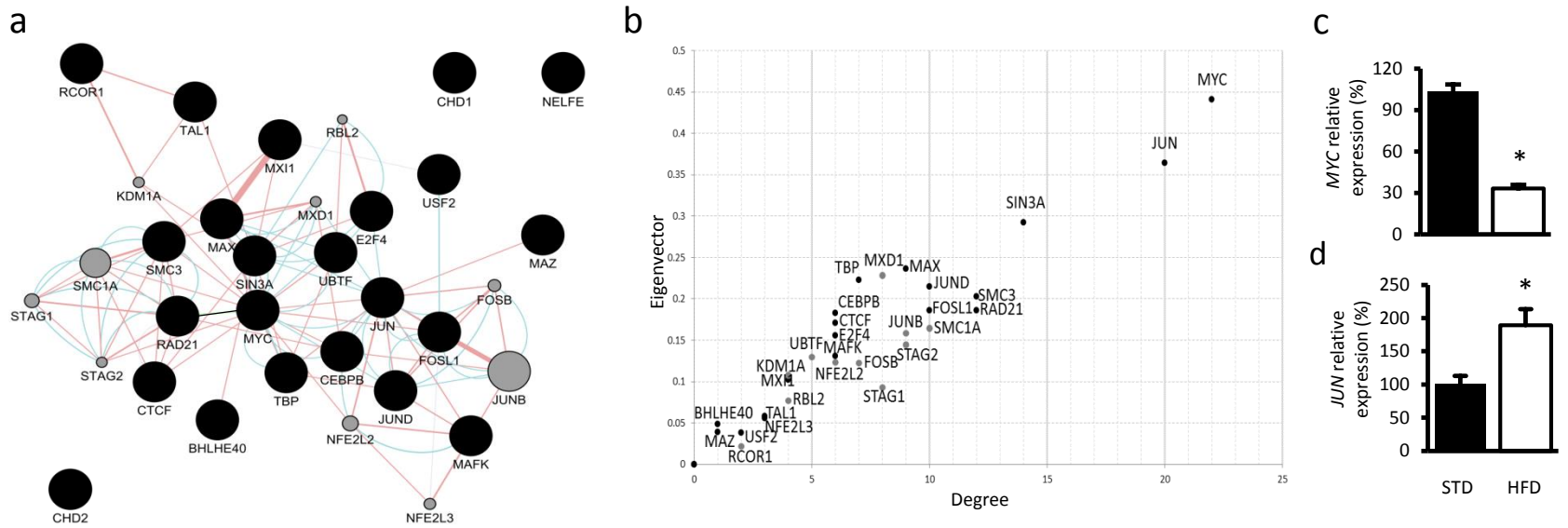
a
RCOR1
TAL1
CHD1
NELFE
RBL2
MXI1
KDM1A
USF2
MXD1
E2F4
MAX
MAZ
SMC3
SMC1A
SIN3A
UBTF
STAG1
FOSB
JUN
RAD21
MYC
FOSL1
STAG2
CEBPB
JUNB
CTCF
TBP
JUND
BHLHE40
NFE2L2
MAFK
CHD2
NFE2L3
b
Eigenvector
Degree
MYC
JUN
SIN3A
TBP
MXD1
MAX
JUND
SMC3
CEBPB
FOSL1
RAD21
CTCF
JUNB
SMC1A
E2F4
UBTF
MAFK
STAG2
KDM1A
FOSB
NFE2L2
MXI1
RBL2
STAG1
BHLHE40
TAL1
NFE2L3
MAZ
USF2
RCOR1
c
MYC relative expression (%)
d
JUN relative expression (%)
STD
HFD

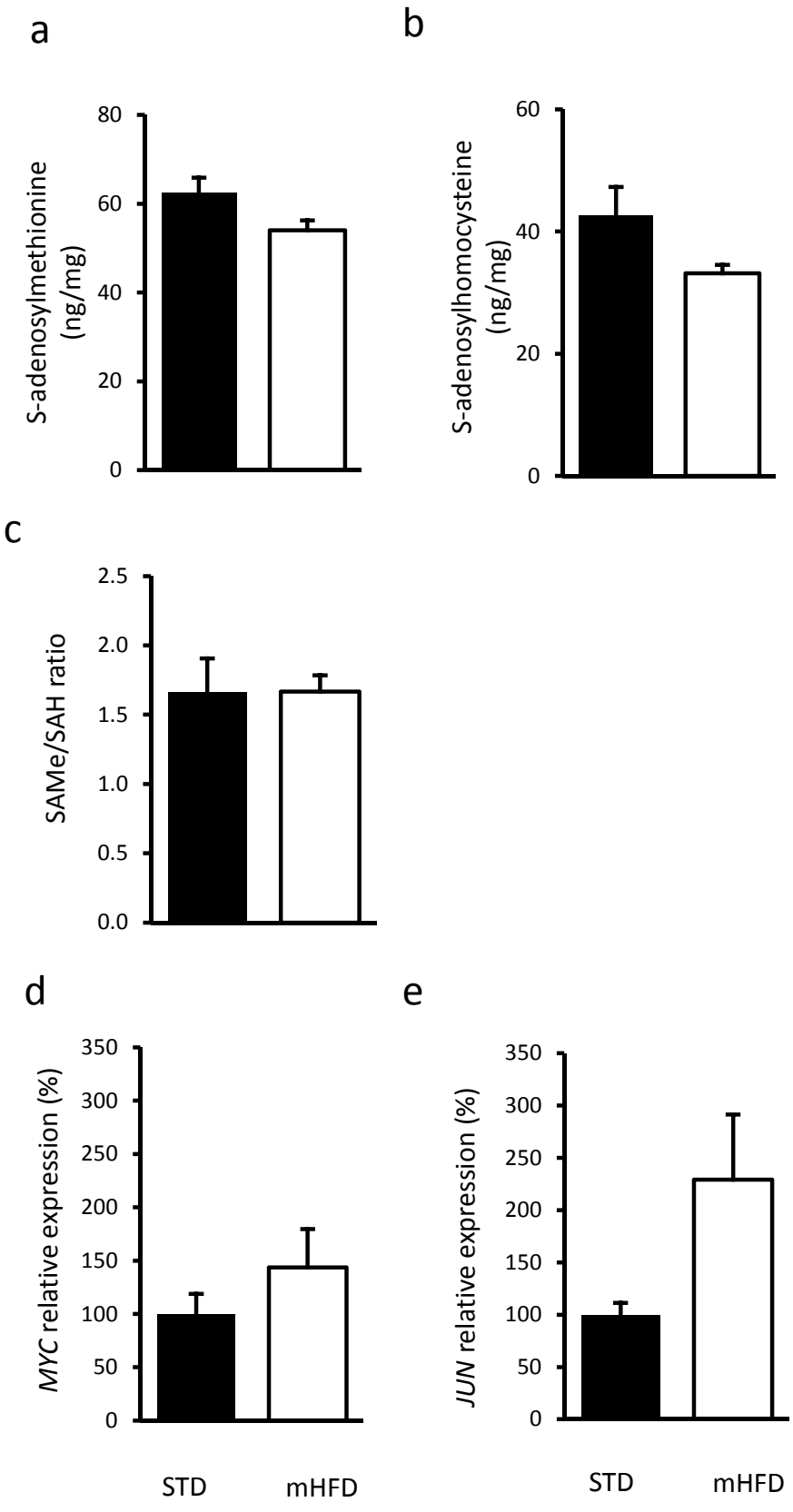
a
S-adenosylmethionine (ng/mg)
80
60
40
20
0
b
S-adenosylhomocysteine (ng/mg)
60
40
20
0
c
SAMe/SAH ratio
2.5
2.0
1.5
1.0
0.5
0.0
d
MYC relative expression (%)
350
300
250
200
150
100
50
0
STD
mHFD
e
JUN relative expression (%)
350
300
250
200
150
100
50
0
STD
mHFD

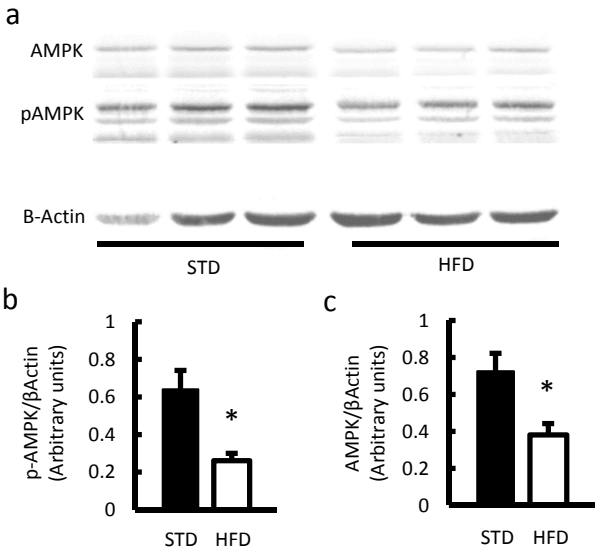
a
AMPK
pAMPK
B-Actin
STD
HFD
b
p-AMPK/βActin
(Arbitrary units)
1
0.8
0.6
0.4
0.2
0
*
STD
HFD
c
AMPK/βActin
(Arbitrary units)
1
0.8
0.6
0.4
0.2
0
*
STD
HFD

SUPPLEMENTARY INFORMATION

Progression of fatty liver disease in hamsters with metabolic syndrome is associated to hepatic accumulation of S-Adenosylmethionine and cell senescence.

Josep Maria del Bas, Benjamín Rodríguez, Francesc Puiggròs, Silvia Mariné, Miguel Angel Rodríguez, David Moriña, Lluís Armengol, Antoni Caimari, Lluís Arola

Supplementary Materials and Methods

Plasma analyses.

Commercial enzymatic colorimetric kits were used for the determination of plasma total cholesterol (QCA, Barcelona, Spain), triglycerides (QCA, Barcelona, Spain), phospholipids (phosphatidylcholine) (Spinreact, Sant Esteve de Bas, Spain), glycerol (Sigma Aldrich Química SA, Madrid, Spain), and non-esterified free fatty acids (NEFA) (WAKO, Neuss, Germany). Plasma lipoproteins were separated with the Hydragel Lipo kit (Sebia, Paris, France) and stained for total cholesterol with the SAS-MX HDL kit (Helena Biosciences; Sunderland, UK). Plasma insulin and leptin levels were measured using a mouse/rat insulin ELISA kit and a rat leptin ELISA kit, respectively (Millipore Iberica S.A., Barcelona, Spain). Adiponectin levels were assayed using a mouse/rat adiponectin ELISA kit (B-Bridge International, Inc, California, USA). Serum AST and ALT were determined with enzymatic kits (QCA, Barcelona, Spain).

Liver histology

For haematoxylin and Eosin (H&E) and Masson's trichrome staining, liver tissue samples were fixed in 4% formaldehyde for 24 hours, dehydrated with a graded series of ethanol (70%, 96%, 100%), cleared with xylene and paraffin embedded at 52ºC using a Citadel 2000 tissue processor (Thermo scientific, Waltham, MA, USA). Two µm thickness sections were obtained with a HM 355S microtome (Thermo Scientific, Waltham, MA, USA) and H&E and Mason's trichrome stainings were performed in a Varistain Gemini ES automated slide stainer (Thermo Scientific, Waltham, MA, USA). For neutral lipid visualization, 10 µm sections of frozen livers were obtained using a Leica CM-3050S

cryostat and stained with Oil red O reagent (Sigma-Aldrich, Spain) and Mayer's haematoxylin solution (Sigma-Aldrich, Spain). Sections were observed with a Nikon Eclipse Ti microscope and micrographs recorded with the Nis Elements software (Nikon Instruments Inc., Melville, NY). Morphological interpretation was done by independent expert pathologists (Eldine patologia, Tarragona, Spain).

Liver extraction and ^{1}H NMR analysis for hepatic metabolite determination

Livers were pooled two by two obtaining 5 STD samples and 5 HFD samples. Pools were extracted as described previously [1]. Briefly, 100 mg of tissue were homogenized in H2O/CH3CN (1/1) solution. After centrifugation (4500 g 25 min at 4 ºC), supernatants were filtered and the remaining pellets were extracted with CH_3CL:MetOH 3:1 v/v . Aqueous and lipophilic phases were separately lyophilized and stored at -80 ºC. For ^{1}H NMR analysis, the hydrophilic extracts were reconstituted in 600 µl of D_2O phosphate buffer (PBS 0.05 mM, pH 7.4, 99.5 % D_2O) containing 0.73 mM trisilylpropionic acid (TSP). Samples were then vortexed, homogenized for 5 min, and centrifuged for 15 min at 14000 × g. Finally, redissolved samples were placed into 5 mm NMR tubes. ^{1}H NMR spectra were recorded at 300 K on an Avance III 600 spectrometer (Bruker, Germany) operating at a proton frequency of 600.20 MHz using a 5 mm CPTCI triple resonance (^{1}H, ^{13}C, ^{31}P) gradient cryoprobe. One-dimensional ^{1}H pulse experiments were carried out using the nuclear Overhauser effect spectroscopy (NOESY) presaturation sequence (RD–90°–t1–90°–tm–90° ACQ) to suppress the residual water peak, and the mixing time was set at 100 ms. Solvent presaturation with irradiaton power of 75 Hz was applied during recycling delay (RD = 5 s) and mixing time. The 90° pulse length was calibrated for each sample and varied from 7.85 to 8.49 □s. The spectral width was 12 kHz (20 ppm), and a total of 256 transients were collected into 64 k data points for each ^{1}H spectrum. The exponential line broadening applied before Fourier transformation was of

0.3 Hz. The frequency domain spectra were phased, baseline-corrected and referenced to TSP signal (δ= 0 ppm) using TopSpin software (version 2.1, Bruker).

NMR Data Analysis.

Data analysis has been described previously [1]. The acquired ^{1}H NMR were compared to references of pure compounds from the metabolic profiling AMIX spectra database (Bruker), HMDB, and Chenomx databases for metabolite identification. In addition, we assigned metabolites by ^{1}H–^{1}H homonuclear correlation (COSY and TOCSY) and ^{1}H–^{13}C heteronuclear (HSQC) 2D NMR experiments and by correlation with pure compounds run in-house. After pre-processing, specific ^{1}H NMR regions identified in the spectra were integrated using the AMIX 3.9 software package.

Hepatic S-adenosylmethionine, S-adenosylhomocysteine and homocysteine analysis.

Methanol, acetic acid and formic acid were purchased to Sigma-Aldrich (St. Louis, U.S.A.). Acetonitrile was purchased to Panreac (Castellar del Vallès, Spain). Analytical standards DL-homocysteine, S-(5'-Adenosyl)-L-methionine chloride dihydrochloride (SAM) and S-(5′-Adenosyl)-L-homocysteine (SAH) were acquired to Sigma-Aldrich.

Samples were extracted as follows: 350µL of 10mM acetic acid H2O/MeOH (1:1) were added to each sample, 5 min of sonication in water/ice, centrifugation at 4ºC 15 min at 13000 rpm. Supernatants were dried, resuspended in 0.1% formic acid H2O/ACN (6:4) and centrifuged at 4ºC 10 min at 13000 rpm. These supernatants were analyzed.

A 1290 liquid chromatograph coupled to a 6490 tandem mass spectrometer (Agilent Technologies, Palo Alto, U.S.A.) was used for the quantification of the 3 compounds. The chromatographic column was an Aquity UPLC HSS T3 (1.8µm x 2.1 x 150mm) (Waters, Milford, U.S.A.).

Mobile phase was A: water 0.1% formic acid and B: acetonitrile (ACN). Injected sample volume was of 2 microliters. Flow rate was 0.4mL/min. Separation was performed at room temperature. The gradient started at 5% B, increased to 10% B until min 1, then increased to 100% of B until min 4 and maintained at 100% B for 2 min. Mobile phase was brought to initial conditions (5% B) and equilibrated for 1 min before the next injection. Total time of the analysis was 9 minutes.

The mass spectrometer was equipped with Electrospray ionization (ESI) and Jet Stream and iFunnel technology. Acquisition was carried out in multiple reaction monitoring (MRM) mode.

For the quantitative method validation calibration curves, linearity, precision, accuracy and method detection and quantification limits were studied, by analysis of a standard dilutions serial prepared in 0.1% formic acid H2O/ACN (6:4) and pooled samples spiked with standard solutions. Method precision was determined from relative standard deviation (RSD%) in the analysis of a spiked pooled sample. Method detection limit (MDL) was defined as the lowest concentration that could be distinguished from a blank. Method quantification limit (MQL) was defined as the lowest concentration giving a linear response.

Hepatic Thiobarbituric acid reactive substances (TBARS) analysis

TBARS were determined as described previously [2] with some modifications. Briefly, a 500 µL aliquot of liver homogenates (10% in PBS) were assayed with 2 mL of thiobarbituric acid (TBA)-trichloroacetic acid (TCA) reagent (0.375 and 15% respectively, Sigma, Spain). Samples were boiled at 95ºC for 30 minutes. After centrifugation (1600g 15 min), 300 µL of the supernatant was extracted with 300 µL of n-butanol (Sigma-Aldrich, Spain) and the samples red at 532 nm. Lysate protein content

was determined by the Bradford assay procedure [3] using a commercial reagent (Sigma, Spain) and following the manufacturer instructions. TBARS were normalized by lysate protein content.

Hamster microarray cRNA synthesis and gene expression analysis.

For Cy3 and Cy5 labeled cRNA synthesis, 100 ng of liver RNA were processed with the Agilent's Low Input Quick Amp WT Labeling Kit (Agilent Technologies, Santa Clara, CA, USA) following the manufacturer's instructions. The resulting labeled cRNA was purified with the Qiagen RNAeasy Mini Spin (Izasa, Barcelona, Spain). cRNA quality, quantity and the Cy3 and Cy5 labeling specific activity were evaluated with a NanoDrop ND-1000 spectrophotometer (NanoDrop Technologies Wilmintog, Delaware, USA).

Since in the microarray the different transcripts are represented by different probes, and each probe is associated to a Log2FC and an adjusted p-value, probe collapsing was carried out with the software R [4]. Briefly; changed genes were selected within those presenting at least a 50% of their corresponding probes significantly changed (Adjusted p-value <0.05). For those, the mean fold-change is calculated and the collapsed adjusted p-value obtained with a Bonferroni based method as described previously [5]. Finally, only those genes with an average adjusted p-value under 0.05 and a mean Log2FC over 0.2 or under -0.2 were considered as up- or down-regulated, respectively. The final list of up- and down-regulated genes is presented in supplementary table 3. Finally, gene expression data was validated by RT-q-PCR analysis of 53 genes (Supplementary figure 5). Passing and Bablock test comparing the microarray and RTqPCR results reported an excellent linear correlation among both methods (pearson's r =0.94) though a significant deviation of both methods was observed. Thus, the intercept value (0.19 with a 95% confidence interval from 0.010 to 0.28) was different from 0 and the slope (0.78 with a 95 confidence interval from 0.61 to 0.97) was different from 1. This was a consequence

of the microarray reporting fold-changes with slightly lower values than RTqPCR. Nevertheless, only one gene followed different regulation tendencies (upregulated in one method and downregulated in the other). Therefore, microarray results were considered to be suitable for our purposes.

Transcription factor binding sites gene set enrichment and subsequent network analysis

For transcription factor binding sites gene set enrichment, significantly changed genes in the microarray were analyzed with the ENCODE ChIP-Seq significance tool [6] using the default options of the software. Since genes in the microarray present the human nomenclature, genes were mapped to mouse genes using the homology mapping from NCBI (http://www.ncbi.nlm. nih.gov/projects/homology/maps) when required. For network analysis, only those transcription factors that were changed in both human and mouse models were used. The plug-in Genemania [7] for Cytoscape 3.0.1 software [8] was used to generate a network in which nodes were the selected transcription factors and edges were either protein-protein interactions (physical interaction option), biological pathway related links (pathway option), gene expression control (genetic interactions option) or co-localization (co-localization option). According to software developers, the information about nodes interactions was obtained from publicly available databases described in [7]. Options to include in the network the 10 most related genes and to calculate inter-relations according to the query genes were selected for the analysis. In order to assess the relevance of each node, the network was further analyzed with the plug-in CentiScaPe [9] in order to quantify the centrality parameters degree and eigenvector, which allow an immediate evaluation of the regulatory relevance of each node within the network.

Supplementary References

[1] Vinaixa M, Rodríguez MA, Rull A, Beltrán R, Bladé C, Brezmes J, et al. Metabolomic assessment of the effect of dietary cholesterol in the progressive development of fatty liver disease. J Proteome Res 2010;9:2527–38. doi:10.1021/pr901203w.

[2] Prabhakar P V, Reddy UA, Singh SP, Balasubramanyam A, Rahman MF, Indu Kumari S, et al. Oxidative stress induced by aluminum oxide nanomaterials after acute oral treatment in Wistar rats. J Appl Toxicol 2012;32:436–45. doi:10.1002/jat.1775.

[3] Bradford MM. A rapid and sensitive method for the quantitation of microgram quantities of protein utilizing the principle of protein-dye binding. Anal Biochem 1976;72:248–54.

[4] R Development Core Team R. R: A Language and Environment for Statistical Computing. R Found Stat Comput 2011;1:409. doi:10.1007/978-3-540-74686-7.

[5] Vovk V. Combining p-values via averaging. arXiv 2012:4966 2012.

[6] Auerbach RK, Chen B, Butte AJ. Relating genes to function: identifying enriched transcription factors using the ENCODE ChIP-Seq significance tool. Bioinformatics 2013;29:1922–4. doi:10.1093/bioinformatics/btt316.

[7] Warde-Farley D, Donaldson SL, Comes O, Zuberi K, Badrawi R, Chao P, et al. The GeneMANIA prediction server: biological network integration for gene prioritization and predicting gene function. Nucleic Acids Res 2010;38:W214–20. doi:10.1093/nar/gkq537.

[8] Shannon P, Markiel A, Ozier O, Baliga NS, Wang JT, Ramage D, et al. Cytoscape: a software environment for integrated models of biomolecular interaction networks. Genome Res 2003;13:2498–504. doi:10.1101/gr.1239303.

[9] Scardoni G, Petterlini M, Laudanna C. Analyzing biological network parameters with CentiScaPe. Bioinformatics 2009;25:2857–9. doi:10.1093/bioinformatics/btp517.

supplementary table 1. Composition of diets according to the manufacturer.

Product #	HFD (D09110401)		STD (D09110402)	
%	gm	kcal	gm	kcal
Protein	23	20	19	20
Carbohydrate	46	40	66	68
Fat	20	40	5	12
Total		100		100
kcal/gm	4,5		3,9	
Ingredient	gm	kcal	gm	kcal
Casein, 80 Mesh	200	800	200	800
L-Methionine	3	12	3	12
Corn Starch	149	596	455	1820
Maltodextrin 10	100	400	75	300
Sucrose	150	600	150	600
Cellulose, BW200	50	0	50	0
Soybean Oil	15	135	15	135
Lard	164	1476	39	351
Mineral Mix S10026	0	0	10	0
S10039, without Selenium	10	0	0	0
DiCalcium Phosphate	13	0	13	0
Calcium Carbonate	5,5	0	5,5	0
Potassium Citrate, 1 H2O	16,5	0	16,5	0
Vitamin Mix V10001	0	0	10	40
V13401, without Vitamin E	10	40	0	0
Choline Bitartrate	2	0	2	0
Cholesterol	4,6	0	0	0
FD&C Yellow Dye #5	0	0	0	0
FD&C Red Dye #40	0	0	0,05	0
FD&C Blue Dye #1	0	0	0	0
Total	892,6	4059	1044,05	4058
Selenium (mg/Kg)	0.07		0.23	

Vitamin E (UI/Kg)	5	50

Supplementary table 2. Oligonucleotide sequences for RTqPCR analysis

gene symbol	**forward 5' → 3'**	**reverse 5' → 3'**
A2M	GGAGCGAAGAAAGAACACTCC	TGGCCTCTTGGCATCTAGTC
ABCA1	TTGGATGGATTATATTGGACTGC	TGGTCTCATTGAAAGCTTCTCTC
ABCG1	CTTCTCCATGCTGTTCCTCATG	GCCAGGTAGTAGGCCTTCAG
ABCG5	CAGCCCAACTCATTCAGGAC	GTGCCACAGAACACCATCTCT
ACADVL	GCAGGTGGAGGAGAAGACTT	TTCTTTCTGGGCCTTTGTGC
ACAT1	AGCAAGATGAAGCCCAGAGA	CCATTGTCCAGAGATGCAGA
ACAT2	GGTGGAATTATGTGGCCAAGA	CATGTTGGCAAAGACAGGGAC
ACSL3	GGGCACCATTAGTTTGCTGT	CCGCTGTCCATTTTCATCTT
ACTINB	ACGTCGACATCCGCAAAGACCTC	TGATCTCCTTCTGCATCCGGTCA
ANGPTL4	CCCCCACACACCTAGACAAC	CTGAGGCTGGATCTGGAAAA
ANXA2	CATGCTGGAGAGCATCAAGA	GCGGGAGACCATGATTCTAA
ANXA3	TGGACCTCGAGGAACCATAA	GCCAGAGAGATCACCCTTCA
APOA5	CCTTACGCAGAACGCTTGGT	TCCTTCGCCTTACGTGTGAGT
APOE	ACACAGGAACTGACGGTACTGAT	GTTCCTCCAGCTCCTTTTTGTAT
ATGL	CACTTTAGCTCCAAGGATGA	TGGTTCAGTAGGCCATTCCT
CPT1A	TCTTCAAAAACAGCAAGATAG	GGGTTGGTTTCTCCTTTACAATG
CTSF	AGTGGCGCTTGACTGTCTTT	TTCCTGACAGGCTCCTTTTG
CYP4A10	CAGGAAGCCCTCACAGGATT	CTGGACCACTTTGAGCAGCA
CYP4A32	GCTCCTTGGATTGGCTATGGT	CAGCATTGACTGGACGGAGT
CYP7A1	ACTGCTAAGGAGGATTTCACTCT	CTCATCCAGGTATCGATCATATT
DDIT3	GACCTGAGGAGCGAGTGTTC	TTTGACTCCCCCTCTTCCTT
DGAT2	TACAAGCAGGTGATCTTTGAGG	GGGCGAAACCAATATACTTCT
FAS	AGCCCCTCAAGTGCACAGTG	TGCCAATGTGTTTTCCCTGA
FDFT1	TGTCCTGATGGTGGAGATGA	GTGAAGATTCGGAAGGGACA
FDPS	GGCGAGTTCTTTCAGATCCA	TTCTGCCCGTAATTGTCCTC
FER1L4	AGGCTCAGGCTGACAAGAAA	CTTTTCTCCCCCTCCCAACT
FGL1	TCAGGTGCAACAGCTTGAGA	AATATTGCCTGGCTCTGGTG
FKBP11	GAGACTTTGGGTCTGCTGGA	GTGTGGGAGAGAAGCGAAGA
FXR	TCTTCAGGAGAAGCATTACCAA	CGCATGTACATATCCATCACAC
GPAT	GCAGACATCTGCTTCACCAA	GCAGGATGATGGGGTTTAGA
GSTM2	GCGGCTGCTTTTCATGTAGT	GCAGGGGACAAGATCACCTA
HACL1	CTGGATGCTGGTACCTTTGG	CCTGCAGATGGTTTCCACTT
HMGCOAR	CGAAGGGTTTGCAGTGATAAAGGA	GCCATAGTCACATGAAGCTTCTGTA
HMGCS1	GTCACACAAGATGCCACACC	CACGTGCCTTCAAAGAGTGA

HPRT	AAGCTTGCTGGTGAAAAGGA	ATGGGACTCCTCATGTTTGC
JUN	GGACCTGCGAGCTTCTTCTC	GACGTCCTGGTAGGAACGC
LCAT	ACACTGGTGCAGAATCTGGTTA	ACTGTCTCATCCCGCACATAC
LDLR	GCATCACACTAGATCTTCCCAGT	GAGTTTGGAATCAACCCAATAGA
LIX1L	GGGGAAGTTGTTTTGGGAGT	GGGCCTCTGAGACACTCTTCT
LSS	CCCTGAACTATGTGGCTCT	ATAGGGTGTTGAGTCCTTCC
MTP	GTCAGGAAGCTGTGTCAGAATG	CTCCTTTTTCTCTGGCTTTTCA
MUG1	AAGGCCACAACAGTTTCCAG	AGGCCAGTGTCTGATTGGTC
MYC	CCCTGACGACGAAACCTTCA	TGCAGGTACAGGCTAGAGGT
PCK1	GGCAACTTACGGGCTATCAA	TTCCTCATCCTGTGGTCTCC
PGLYRP2	AGCTTCAAGCCCTGATTTCC	AGACGGCTCCAGTGTTTGTC
PPARa	GTGGCTGCTATAATTTGCTGTG	AGCTTCGGGAAGAGAAAGGTAT
RCL1	ATGAAAGGCGTCAACTCTGG	AGGGTCATGAGCAGCAGAAC
REEP6	GGGTGGTGTACGCTCTGTTC	GTCCAGAGCCATGTGGTGTT
SAA3	ACTATGATGCTGCCCAAAGG	GTCGGAAGAAGTTGGGGTCT
SERPINF1	ATCCAGCTTTGTTGCACCTC	GCTGATAGCACTGGGCATTT
SLC26A6	TGTGAGCTGCTCCATGTCTC	ACTCGATTTGCCTTCCACAG
SLC27A2	CAAGTTTTCAGCCAGCCAGT	TTCGGTGGAAGCGTAGAACT
SRBI	TCCCACCTTTGAGAAG	TGATGTCCAGCCGTAT
SREBP1	GCGGACGCAGTCTGGG	ATGAGCTGGAGCATGTCTTCAAA
SREBP2	GGAGAATGGAGGGGTCACAA	GCAGCCAAGGAGAGTCTGTA
TBP	GACAACTGCGCTGATTTTCA	CAGCCTTATGGGGAACTTCA
THRSP	ATCACCACCTGCTCCATGTT	GCTTTGGCATCCTGTCAATC
UBE2L6	AGCAGCTACAAAGGGAAGCA	TTCAGGAGGAAGGCAGAAGA
WSCD2	AAGCTGGGTGCTGTTCTGTC	GCTCAGGAGGGCAGTGTAAG

Supplementary table 3. Upregulated and downregulated genes according to the microarray

GeneName	logFC	adj.P.Val
UPREGULATED		
ABCG5	2.89553353	1.34E-15
FER1L4	2.77222607	1.22E-19
RSAD2	2.3776297	1.47E-07
GPNMB	2.358390769	1.37E-10
MLF1	2.205077627	8.15E-06
WSCD2	2.194201354	1.18E-16
GCK	2.120779591	1.62E-12
ANXA2	2.075817318	5.99E-20
ANXA3	1.913207648	5.25E-19
ANKRD2	1.882260502	5.61E-11
FST	1.873094376	1.92E-10
TMEM171	1.809132641	5.34E-10
CES1F	1.723301848	2.66E-09
A_Chain_A._Crystal_Structure_Of_Human_P53_Inducible_Oxidoreductase_(_Tp53i3.Pig3)	1.660464399	7.26E-09
GSTM2	1.589475788	2.39E-21
INMT	1.526347803	3.54E-20
SLC4A5	1.520229173	3.30E-07
CLCA1	1.512937059	2.01E-06
DYNC2LI1	1.496261802	4.52E-07
FADS6	1.493349866	1.10E-08
USP18	1.490255937	6.15E-13

TRPC6	1.482035837	6.67E-13
TM4SF19	1.477262472	1.02E-11
TC2N	1.457726011	1.07E-06
LIX1L	1.4467715	7.70E-16
ABCG8	1.384677317	5.97E-09
GCAT	1.37237091	3.13E-14
CYP4A10	1.349949075	1.18E-14
IFIT2	1.319344602	9.30E-05
2810432L12RIK	1.312164183	3.09E-07
ALPK3	1.301812236	1.73E-06
NME5	1.282004831	1.20E-07
SREBF1	1.275871608	9.42E-14
UAP1L1	1.275002745	5.36E-09
STEAP4	1.267682032	7.47E-14
PPM1J	1.267011517	8.58E-05
LGALS3	1.266475152	4.82E-08
ANGPTL3	1.261926196	7.98E-11
TRPC1	1.25166932	0.001203798
SDC1	1.246381114	6.51E-09
TSPO	1.236178069	0.00225
TUBA8	1.19412442	2.98E-10
legumain_precursor_[Mus_musculus]	1.18067813	3.07E-17
CLCA4L	1.177686539	2.42E-07
CHCHD10	1.175468595	2.90E-10
UBE2L6	1.175069967	2.02E-17

4933404M02RIK	1.169930402	1.63E-05
GPR137B	1.162248233	9.45E-07
IFIT1	1.159652903	8.52E-08
PARP12	1.146490549	3.37E-12
FGF1	1.12732707	5.60E-05
NLRC3	1.123418637	1.86E-08
CYP4A1	1.121821921	3.46E-13
SLC15A3	1.110118612	2.70E-09
CYP4A32	1.106619104	1.66E-16
SLC26A7	1.104077959	0.001227714
CTSA	1.099304124	2.60E-15
PLIN3	1.088953873	0.000214
PRODH	1.088430289	3.21E-11
WFDC2	1.087987919	1.23E-09
DOCK7	1.084500448	1.50E-05
ETV1	1.082752518	2.83E-08
GSTT3	1.076256943	6.58E-10
GM6484	1.075336035	1.73E-08
GNPDA1	1.074503863	1.72E-12
TUBGCP3	1.067485993	1.04E-15
GDF15	1.057771482	1.50E-07
LMBRD1	1.045084429	4.52E-08
CLIC5	1.038354977	7.04E-09
PLAU	1.033744075	2.41E-07
GPR160	1.008362324	2.17E-11

9030224M15RIK	1.001005843	1.69E-07
MYLIP	0.996760909	2.24E-09
PPP1R3C	0.990611806	8.56E-07
TXNRD3	0.985848849	5.34E-09
TCN2	0.984608961	4.46E-09
ANXA5	0.966801484	1.54E-07
ODF3B	0.959347038	0.000495
CES1C	0.935753959	5.36E-16
FMO3	0.934032126	1.13E-10
WNT5B	0.933866549	9.69E-06
3110003A17RIK	0.933796054	2.19E-12
LOC498276	0.932635754	8.18E-09
RHOQ	0.93236772	3.40E-15
SH3BGRL	0.927319383	1.20E-08
CCDC138	0.926045871	1.25E-05
9030625A04RIK	0.924966976	1.06E-09
GRAMD1C	0.924090798	6.06E-11
SCPEP1	0.924062539	0.020764578
TRIB3	0.919651496	5.11E-10
TRIM37	0.907967517	4.30E-06
RAB20	0.907368686	3.45E-10
CTSK	0.905303945	1.04E-10
RND2	0.897023877	1.08E-08
CBG_MESAU_RecName:_Full=Corticosteroid-binding_globulin;_Short=CBG;_AltName:_Full=Serpin_A6;_AltName:_Full=Transcortin;_Flags:_Precursor	0.891116276	2.79E-12
CYP20A1	0.889888489	4.48E-08

SERPINB1A	0.889331288	2.44E-11
TMOD1	0.883221872	1.81E-05
TGFBR1	0.873387226	2.53E-07
C12ORF48	0.86851515	3.15E-05
GNS	0.861184371	1.33E-10
RENBP	0.858482232	9.68E-08
BLVRA	0.858059292	1.34E-06
CLEC4F	0.851407	9.44E-10
PPT1	0.846046333	4.79E-05
IRF7	0.836081575	2.75E-13
THRSP	0.835927437	2.33E-15
LDHB	0.833958897	7.56E-10
RAB31	0.830515213	0.001132
GPRIN2	0.823807437	1.19E-08
CD63	0.823120311	2.70E-11
FCRLA	0.821452802	3.42E-08
SERPINB6A	0.8173981	1.91E-13
CABLES1	0.816993498	1.49E-08
SERPINB8	0.816651694	4.08E-09
APOBR	0.811868787	0.000195
CD68	0.808773736	1.08E-09
NIPAL2	0.808458303	5.80E-08
CYP4A12B	0.80842911	3.56E-07
IDH2	0.808387473	1.45E-11
RRAGC	0.80672788	4.37E-06

TMED3	0.80140 1021	6.65E-07
GBP3	0.80084 3285	9.84E-08
FAT1	0.79627 1872	3.58E-05
CCL24	0.79289 2429	7.56E-10
DDIT3	0.78944 2219	1.92E-07
PION	0.78889 9933	1.24E-06
GM1661	0.78590 994	1.18E-07
FHIT	0.78389 8244	9.82E-10
LAPTM4B	0.78360 095	1.09E-09
THADA	0.77643 7159	0.00027 18
SETD7	0.77480 6098	3.21E-05
KIAA1598	0.77162 6404	8.58E-05
1700029I01RIK	0.76283 6577	3.38E-07
MFSD1	0.76235 9694	4.20E-09
0610010F05RIK	0.75905 1276	8.70E-05
TREM2	0.75723 4926	3.12E-05
TTLL7	0.75723 1412	3.70E-07
UPP1	0.75606 384	8.97E-06
TPI1	0.75568 3262	3.74E-08
SULT1C2	0.75539 2892	7.10E-05
ALDH9A1	0.75063 7346	4.08E-10
GSTM3	0.74863 3665	1.91E-11
KLHL7	0.74677 7228	5.52E-05
TNFRSF12A	0.74655 0731	2.64E-09
NAIP5	0.74622 2647	0.00872 3529

IRAK1BP1	0.745317146	0.001380212
5033414D02RIK	0.744122359	3.27E-07
PALM3	0.742180815	5.72E-07
RASA2	0.740886915	6.99E-09
PDGFA	0.740492236	1.04E-06
ARL4C	0.739370111	0.000666
OASL	0.73820641	1.19E-10
GYPC	0.733598635	1.12E-09
SPC24	0.729943	1.09E-09
E430025E21RIK	0.727757161	2.11E-08
PSAP	0.723831174	1.89E-07
D6WSU116E	0.723462794	1.32E-06
SLC19A2	0.721384684	1.54E-09
APOA4	0.72038936	0.005205519
AMDHD2	0.720320796	5.00E-10
SPI1	0.720067313	1.75E-06
FXYD6	0.71519209	5.96E-08
MLKL	0.711129825	3.46E-06
CD53	0.709968346	4.95E-08
DPP7	0.700178289	1.37E-07
GM13251	0.699565312	9.83E-06
DDX60	0.699491669	0.00152
RNF145	0.698818732	1.41E-05
GALK2	0.697727033	1.50E-09
DRAM2	0.697427573	3.99E-05

FAM105A	0.696955007	6.40E-05
CLDN2	0.69653479	1.05E-07
TAGLN2	0.696151499	1.73E-09
MANBA	0.695253735	0.000965
RILPL1	0.693761426	5.61E-09
SERPINB9	0.693582974	1.67E-10
5730409E04RIK	0.691686324	0.0001082
MARCO	0.691168256	3.07E-10
TSPAN4	0.685200601	2.38E-11
OASL1	0.684037706	1.65E-07
CRYL1	0.683355921	4.80E-11
CDK1	0.681464542	1.57E-08
GLDC	0.681111904	9.85E-10
HGD	0.68064696	0.0004335
MFSD7A	0.680595434	2.18E-05
TSKU	0.678521657	1.60E-09
GRAMD1B	0.675717953	4.14E-09
CTSZ	0.673446775	3.35E-11
NQO1	0.673158085	0.000594
LOC500959	0.671440291	1.35E-10
BMP2K	0.670270522	2.92E-05
STX3	0.668244049	2.23E-07
KIAA1841	0.667472736	1.73E-05
LGALS3BP	0.666965173	1.03E-06
COMMD4	0.666861393	1.76E-09

GNB4	0.666033607	7.56E-05
GINS1	0.665971717	0.000344
anti-mouse_CD3_receptor_immunoglobulin_light_chain_variable_region_[Cricetinae_gen._sp.]	0.665536281	8.01E-07
GBP9	0.665066165	1.39E-09
HCK	0.664915073	1.64E-07
SIRPA	0.664378254	3.46E-13
RNLS	0.66431472	1.48E-06
GBP5	0.66155206	1.61E-06
TUBB2B	0.659618446	4.58E-10
PDXK	0.658686052	5.84E-08
RHOC	0.653804598	1.38E-06
RTN4IP1	0.650677645	2.86E-06
CYP4V3	0.650134926	2.34E-06
CYLD	0.648999147	0.001025
TWF1	0.648820501	1.87E-10
SCNN1B	0.646602078	2.04E-08
GBP10	0.646221866	0.000999
GBP8	0.645079366	3.02E-06
TPX2	0.644814921	1.24E-05
TMEM106B	0.644797989	8.55E-05
ANK	0.643857538	1.21E-05
ARSA	0.638168707	1.58E-09
BTBD8	0.637317307	0.00283
PLA1A	0.636067165	1.02E-11
MOCOS	0.63595473	4.20E-08

CASP6	0.635885778	3.58E-09
DENND4A	0.634005525	0.0001428
DYNLT3	0.633873248	3.18E-06
TRIM45	0.633738297	8.85E-07
LOC688090	0.630849715	0.00503972
P2RY6	0.62596666	1.35E-09
PLEK	0.623577361	0.0001408
SAMD9L	0.621620936	0.000462
RGS5	0.620501042	0.000128
CCS	0.620147533	1.92E-07
DCP2	0.61961817	6.61E-08
RGD1310552	0.619510276	1.54E-07
AOAH	0.618571397	3.18E-05
PITRM1	0.618479302	2.03E-05
PPP1CB	0.618362788	1.85E-06
GBP4	0.61799229	1.10E-05
CCDC34	0.614069288	1.35E-09
SNAPIN	0.613580735	2.72E-06
GNGT2	0.613368799	1.69E-11
AKAP17B	0.611466715	0.002050924
CYP3A23/3A1	0.608972396	1.18E-08
NINJ1	0.608215734	0.000286
DDC	0.604957283	1.44E-11
ZFYVE21	0.601831913	4.14E-11
STMN1	0.598432093	5.61E-07

MARCH9	0.593077415	0.000984
ETNK1	0.590869772	2.86E-07
PRPS2	0.590370155	0.00026
ARL6IP5	0.589636895	8.40E-07
PLOD1	0.586327742	1.13E-05
NAGK	0.582694988	7.55E-07
MDFIC	0.581710476	7.92E-05
CDKN3	0.581584281	1.92E-06
DSN1	0.580409754	0.000101
CAST	0.5797986	3.00E-06
DAB2	0.576875918	1.37E-10
TLR4	0.576730085	3.90E-05
KCNIP3	0.576598198	2.03E-07
ACYP1	0.575996809	2.94E-09
CTSC	0.573813766	3.21E-11
UNC13A	0.573044427	1.60E-07
B3GNTL1	0.573028316	2.08E-05
BCL2A1A	0.572591893	2.96E-07
MCCC2	0.567769954	1.37E-07
MLXIPL	0.567347441	2.46E-08
TP53BP2	0.565487014	5.82E-07
ACTG1	0.560115648	2.00E-12
FMNL2	0.557767246	3.68E-06
SDC3	0.555873962	2.23E-06
EXOC4	0.555460973	2.84E-09

CS	0.555075717	3.00E-07
MFSD7	0.552475505	6.04E-05
SPG11	0.551234872	0.0001224
TRPV4	0.548029391	7.21E-06
UGCG	0.546148722	5.37E-12
TMEM120A	0.545202628	2.78E-07
LY86	0.541511422	2.68E-06
TMEM188	0.540873686	2.19E-06
APPL2	0.539688403	2.12E-05
ATP6V1B2	0.538693315	6.89E-11
C5ORF25	0.537605568	3.49E-05
TEX264	0.537022369	6.48E-08
ZFP775	0.5369162	5.37E-07
STX8	0.536469128	2.43E-05
ADSSL1	0.53598113	5.01E-09
CTSD	0.535095219	2.72E-09
TRIM55	0.534119004	0.011694018
PSTK	0.532541858	6.30E-07
HFE	0.530913838	0.003031241
GSTP1	0.529431382	9.98E-07
CKB	0.528937828	1.81E-08
DGAT2	0.528165784	3.58E-10
RT1-CL	0.527630788	6.63E-07
RT1-CE4	0.52729513	2.32E-06
CYP3A44	0.526092277	3.72E-08

ASB13	0.525700559	2.84E-05
LOC100130890	0.522927371	9.35E-06
RNF135	0.522035611	4.49E-06
STAM	0.519699619	7.70E-10
AGPAT5	0.518957016	5.79E-07
DPP4	0.518937176	7.42E-08
NRBP	0.517803946	1.54E-09
4930506M07RIK	0.517230176	4.24E-06
AGTRAP	0.516957169	6.87E-05
TEP1	0.514981339	1.97E-05
CMPK2	0.514461044	0.005074284
ZNF295	0.514388747	0.000121
RT1.AA	0.513337072	9.87E-08
TMEM86A	0.512347651	1.02E-06
CXADR	0.512120441	3.87E-08
GBP11	0.511418682	2.78E-10
TMSB4X	0.510719538	3.48E-05
LZIC	0.510317174	0.000292
QSOX1	0.509612033	6.97E-05
MAP3K1	0.508963959	1.89E-08
ABI3	0.50855391	4.44E-05
SERAC1	0.508434644	0.000126
GGA2	0.50619399	1.00E-09
DYNLL2	0.506183091	5.46E-09
E2F8	0.505043351	0.003524417

SLC13A3	0.503932777	4.67E-08
HSD17B11	0.503368558	2.17E-05
2410066E13RIK	0.503334824	4.22E-05
HERC2	0.503094849	6.21E-06
H2-Q10	0.502809147	5.52E-06
LOC691909	0.501812533	0.000101
HAUS4	0.499116383	0.0036
SLC6A20A	0.497786296	3.36E-05
VAV1	0.497721536	2.17E-09
DSG2	0.497067151	1.48E-09
MOBKL1B	0.496759567	2.53E-07
PEPD	0.495271864	2.11E-09
PEX11G	0.494289842	1.36E-08
APOE	0.494178187	8.94E-10
HLA-B	0.492708547	7.71E-07
RGD1303130	0.491959491	6.44E-05
PHLDB3	0.490492924	3.33E-09
MYL6	0.48991629	2.94E-05
TXN1	0.487927913	2.83E-09
RT1-CE13	0.487210305	7.34E-06
KIAA1107	0.48683561	3.94E-08
NCF2	0.486171089	1.68E-07
PREDICTED:_copine_II_[Rattus_norvegicus]	0.485212674	9.09E-05
SERF1	0.484171214	1.24E-08
CDKN2B	0.482124971	1.90E-07

DSCR3	0.478234428	1.99E-08
FTH1	0.477506365	5.12E-08
IFI27L2A	0.477016247	2.53E-14
PSMB8	0.47593182	2.06E-07
EML4	0.4755425	1.68E-06
GTPBP8	0.474218437	0.024760358
LONP1	0.472856297	4.18E-09
PSMB10	0.472544137	4.88E-06
ARL6IP1	0.4720686	7.46E-10
ITGAV	0.471117709	3.81E-07
HEATR7A	0.471093284	1.48E-05
RAB7A	0.470988166	8.82E-09
SCD2	0.469503518	5.71E-12
BCAR1	0.469110453	1.07E-05
KRT8	0.46835347	8.36E-05
ANKRD12	0.46781892	0.0001974
GLA	0.466405138	1.56E-05
SCD1	0.464385103	3.34E-13
PEX11C	0.463270814	2.59E-09
RGD1563982	0.463152758	4.49E-07
CCNB1	0.458572871	0.008879425
PPA1	0.458540048	5.11E-09
TUBB2A	0.457400412	9.05E-09
MAPK9	0.457355876	3.07E-08
DUSP22	0.454568403	1.60E-07

SEC14L4	0.45370 1372	8.88E-06
GBP6	0.45342 8331	6.34E-10
USP20	0.45322 2974	4.90E-08
PWP1	0.45313 3172	3.81E-06
CCDC109B	0.44898 6666	6.20E-05
GUSB	0.44843 399	4.89E-06
GFM1	0.44685 2618	1.58E-07
POR	0.44662 8311	0.00020 4
ONECUT2	0.44476 9523	4.19E-07
DYNLT1E	0.44432 7676	1.84E-06
UGT2B	0.44339 717	7.93E-05
RASSF8	0.44272 7505	2.72E-07
GSTM1	0.44170 4157	1.74E-10
NEK3	0.44043 7681	9.81E-07
LOC688495	0.44039 8414	1.47E-05
C5ORF4	0.43998 6276	4.58E-06
NAPA	0.43995 3612	2.69E-07
FUNDC1	0.43820 7648	3.16E-06
SCD4	0.43746 8105	3.84E-10
CTSL1	0.43711 7872	5.80E-06
CREG1	0.43642 1094	1.51E-08
ARHGAP12	0.43555 2087	2.45E-05
ATP11A	0.43546 1911	4.98E-10
UGT2B35	0.43452 6562	1.02E-05
MAP4K1	0.43416 9832	1.64E-05

SH3BGRL2	0.43409 0305	3.66E-06
AOX3	0.43319 2314	5.42E-07
PPM1H	0.43249 0236	1.14E-05
0610031J06RIK	0.43220 0792	0.00010 95
SKA2	0.43219 3648	0.00024 87
CFP	0.43108 3872	2.05E-09
RT1-CE7	0.42940 4027	9.75E-07
ZSWIM7	0.42711 5762	6.85E-08
NRG4	0.42675 7743	5.70E-12
NSMCE2	0.42656 3806	9.98E-09
H2-M3	0.42630 0155	2.52E-06
SIAT7F	0.42369 2436	0.00989 6515
RT1-CE16	0.42315 4786	1.29E-05
LYRM7	0.41916 5171	6.56E-06
MYL12B	0.41839 6757	3.75E-05
SMPDL3A	0.41742 3268	3.56E-07
DCDC2A	0.41704 5782	3.94E-08
GBP1	0.41483 4122	1.15E-07
ZMPSTE24	0.41462 7044	6.08E-06
FAF2	0.41346 8784	3.82E-07
DDAH2	0.41333 7331	0.00401
ACOT13	0.41317 5901	5.32E-10
DNASE1L3	0.41222 7232	1.13E-09
ADAP2	0.41188 3557	9.78E-05
NAGA	0.41175 6344	2.09E-08

AADAT	0.411356845	1.69E-08
ARF2	0.41021901	1.60E-05
NQO2	0.409966726	1.58E-07
MYL6L	0.407824343	2.19E-07
NAGLT1	0.406649512	2.34E-05
PLDN	0.406626974	0.0001888
GIPC1	0.406151606	2.81E-05
IGFALS	0.404188436	2.13E-07
HN1	0.403680706	0.000351
FAM164C	0.402583896	0.00316
RNASEL	0.40171648	0.008971155
6330416G13RIK	0.399660949	4.04E-07
KIAA1217	0.399305374	0.00036
GM8909	0.398686114	2.68E-05
AQP8	0.398051467	9.84E-06
MCCC1	0.397241064	6.02E-06
CLIC4	0.39703675	0.000969
GPT2	0.392743198	5.35E-08
UBE2F	0.392045963	1.29E-05
ADHFE1	0.39116862	1.77E-06
FBXO18	0.391135478	0.0002235
MND1	0.389702603	0.000106
ATP6V1F	0.389342534	3.13E-06
IGHM_MESAU_RecName:_Full=Ig_mu_chain_C_region	0.385189406	3.22E-05
GNG2	0.384776565	7.68E-07

BAX	0.380598018	0.005396751
SLIT2	0.37924913	0.028447887
TMEM111	0.376860823	1.92E-07
RT1-DMA	0.376336799	0.001238221
DNAJC13	0.375942577	4.56E-06
GM11127	0.374565228	1.60E-06
IPMK	0.373217885	0.0010884
SQSTM1	0.372601163	3.40E-07
ELTD1	0.372070067	4.91E-05
CFHR1	0.369383646	1.43E-05
LOC100188936	0.364370219	0.000157
CFL2	0.364093102	1.45E-05
H2-T23	0.363798037	3.96E-08
FBXW4	0.3626967	0.000548
NTPCR	0.360004914	4.16E-05
ADPRH	0.35892218	4.77E-05
RGD1563706	0.35811681	2.28E-05
DPYS	0.354405759	7.74E-09
NIPSNAP1	0.351480986	9.57E-08
TUBB6	0.350894113	6.39E-07
SDHB	0.350247038	7.50E-05
MCOLN2	0.350007169	0.000101
DUSP19	0.3492121	8.55E-06
TOP1MT	0.348256279	1.30E-07
AI413582	0.348232244	0.003703992

LOC691083	0.34752 3425	0.00052 2
SNX4	0.34752 294	0.00018 48
TAPBPL	0.34702 7376	1.87E-05
HBP1	0.34573 9135	0.00031 4
LOC682999	0.33988 525	0.00300 3072
GM4841	0.33896 4167	2.35E-05
1700112E06RIK	0.33712 939	8.73E-07
SLA	0.33560 8027	1.60E-06
SCD3	0.33402 9769	6.84E-13
HIST1H2AN	0.33393 5968	1.47E-07
CYB561D1	0.33379 8374	0.00078 4
LOXL2	0.33277 2602	9.05E-08
VDAC2	0.32992 1844	0.00042 12
AKR1C1	0.32917 415	3.08E-08
STOML2	0.32794 524	2.43E-05
STRADA	0.32750 9738	0.00248 9183
CML2	0.32700 912	7.06E-09
RGD1309437	0.32693 911	1.98E-06
DGCR6	0.32615 8494	3.94E-06
0610010O12RIK	0.32526 1593	0.00047 2
LEAP2	0.32404 7341	3.99E-07
CNDP2	0.32403 0528	0.01290 526
HIST2H2AB	0.32097 8315	1.12E-06
Mouse-PGK1_3	0.32007 4952	2.80E-08
SHROOM1	0.31981 6294	0.00040 95

1110003E01RIK	0.318713431	0.000344
RDX	0.317949914	5.59E-07
SERPIND1	0.31793043	2.04E-06
AKR1A4	0.316342639	6.08E-06
THOC3	0.31533611	4.36E-07
MTHFS	0.31479574	3.50E-06
HIST1H2AE	0.312543556	1.60E-07
HIST1H2BQ	0.312132275	1.58E-06
CFD	0.311402414	4.92E-08
CXCL1	0.310089295	3.04E-11
ARPC3	0.306469764	0.000289
GTSE1	0.304454155	0.000626
RT1-CE12	0.302722277	9.43E-06
CBR1	0.302629382	4.04E-07
CYP4F3	0.298224061	0.006330368
PIGY	0.294920651	2.02E-05
Human-PGK1_3	0.294334694	5.27E-08
UGT2B36	0.294098768	2.31E-07
RGD735175	0.293988211	2.77E-06
RGD620382	0.293383588	3.92E-06
ALG5	0.290123428	6.57E-05
ARHGAP22	0.290087011	0.003080877
C4A	0.289282394	3.33E-08
CLIC1	0.288411185	5.97E-06
SDHA	0.287064408	2.80E-05

TBCB	0.2867141	6.96E-06
AP4S1	0.28577498	1.03E-07
NDUFB7	0.281133469	4.66E-06
1700047I17RIK2	0.279898144	8.22E-06
PRELID1	0.279993857	2.21E-07
SAT2	0.277755059	9.15E-06
SULT1B1	0.27730151	0.0002336
CYP4A8	0.276891406	5.95E-12
CES2F	0.275403925	3.94E-06
TMEM9B	0.271260309	8.96E-06
SLC21A4	0.270584598	0.000408
UFSP1	0.26897162	0.001090172
DNAJC11	0.267536472	3.00E-07
FGFR1OP	0.266978672	0.000477
DYNLRB1	0.263006875	1.20E-05
SELENBP1	0.262566499	1.29E-08
CML1	0.261708178	4.61E-10
GNG12	0.259504179	0.0001122
PQLC2	0.259082569	2.50E-05
THNSL1	0.258260952	1.57E-05
TXNDC17	0.252046212	1.98E-05
DOWNREGULATED		
FABP5	-0.202188056	5.18E-05
DDX24	-0.20524236	0.000938

RPS13	-0.215181418	0.000232
CKS1B	-0.228181883	2.66E-05
KNG2	-0.235447281	8.13E-06
MSMP	-0.236694677	1.73E-08
GM13611	-0.239280422	0.00573111
PLA2G2A	-0.24252336	8.19E-08
EG214403	-0.244382001	0.001572208
BC026782	-0.251256669	7.17E-05
CYP2C29	-0.253658485	3.27E-07
PXMP4	-0.253984709	1.19E-07
F2	-0.257243267	0.000974
LOC293989	-0.2601916	1.66E-07
PEX16	-0.262371383	0.000813
NR4A1	-0.265842775	8.33E-12
AB099516	-0.272878002	0.001412
EBI3	-0.276456973	9.80E-06
SPCS3	-0.278240105	6.72E-05

TMEM220	-0.278889197	0.00655
ECI1	-0.279875492	1.51E-07
FAM13B1	-0.284410388	5.91E-05
RPS18	-0.288551913	5.80E-06
DNAJB11	-0.289096666	1.19E-05
WDR74	-0.290355923	0.0003384
EIF4EBP3	-0.292112795	0.010637798
F12	-0.301334402	2.95E-07
ENY2	-0.302249312	0.0002985
POLR2I	-0.30336909	0.00398
PAIP2B	-0.304149026	8.16E-05
ACOT12	-0.317793464	9.84E-06
GM16378	-0.321387644	1.97E-07
INSRR	-0.322828155	1.77E-06
LOC690728	-0.322831265	1.17E-05
MFSD2A	-0.322924241	9.94E-05
IFT20	-0.323735766	0.033081845

CIB2	-0.331028118	2.66E-08
MGP	-0.33294478	3.14E-09
CCDC55	-0.334311536	0.000117
MGC94190	-0.335166245	8.76E-05
DNAJC21	-0.337431626	0.00062
SEC23B	-0.337486639	3.74E-05
Rat-GAPDH_5	-0.339180347	1.36E-06
2810459M11RIK	-0.340084894	0.0001384
ITIH3	-0.345545802	9.28E-06
RGD1306576	-0.347270263	3.28E-05
ISPD	-0.348299999	1.44E-05
HNRNPH3	-0.349829806	6.75E-05
EIF5	-0.35062826	0.003036
SERPINF2	-0.35068708	4.78E-07
GRB2	-0.352205171	0.027550775
DNAJC12	-0.35903118	6.56E-09
GALE	-0.364671594	9.36E-06

DBNDD2	-0.365598495	1.81E-08
SDS	-0.366228434	1.50E-09
PGM3	-0.36658874	0.010978246
CYP2C68	-0.366871306	9.72E-10
LTF	-0.367374753	3.94E-10
SEC61A1	-0.368266905	7.54E-06
CYP2C18	-0.368328549	3.32E-08
CYP2C37	-0.369944337	1.90E-07
RTDR1	-0.374430563	0.002794382
PPCS	-0.376466662	0.0193
GK	-0.377140204	0.007271216
MYH6	-0.377277536	0.000221
4933424B01RIK	-0.377915514	4.36E-06
SERPINA3M	-0.379058961	2.19E-05
INPP1	-0.380377516	3.02E-07
NPC1	-0.380377808	1.44E-05
MBL2	-0.381300527	5.88E-05

NRP1	-0.382822427	6.36E-05
APOH	-0.383182942	3.33E-08
CCDC24	-0.384051472	1.29E-09
SLC23A1	-0.384813202	4.22E-05
DYSFIP1	-0.384955258	0.00167142
RPL7L1	-0.385041664	4.80E-05
RPN1	-0.386454339	3.58E-06
PEX14	-0.386997563	0.0001064
CARHSP1	-0.391263435	1.30E-09
LRRC59	-0.393340676	6.00E-04
CPT1A	-0.393374779	1.85E-07
FBP2	-0.39355232	1.19E-09
PPIC	-0.396700251	8.76E-07
GPR146	-0.39723125	2.51E-06
OAT	-0.399824309	1.16E-05
FITM2	-0.401306816	1.36E-06
SULT2A7	-0.403145503	1.09E-06

ID2	-0.405591067	1.77E-06
PAQR9	-0.406258432	1.94E-06
SSU72	-0.406809404	3.98E-10
PPAP2A	-0.408848708	1.72E-09
OPLAH	-0.412998448	2.13E-09
Mouse-GAPDH_5	-0.413457596	4.53E-05
HBB-B1	-0.414877983	3.56E-12
IKBIP	-0.415136744	2.70E-05
HAND2	-0.415938965	9.02E-06
ADCK5	-0.416856869	7.29E-07
TMEM5	-0.419426536	6.18E-07
SNRPC	-0.41980247	0.006021367
ZFP677	-0.420562502	7.08E-09
CYP2D4	-0.420712756	3.43E-08
BTD	-0.422420719	1.67E-06
RASGEF1B	-0.42448646	1.40E-05
SH2D4A	-0.42880008	9.95E-10

SDC4	-0.429264243	2.35E-09
PL-5283	-0.429446948	7.85E-07
LYC2	-0.429769534	1.17E-08
RPL39	-0.430109034	0.002317213
GPD2	-0.432480512	5.82E-10
4921524J17RIK	-0.433186275	8.24E-05
PEX1	-0.433910831	2.77E-07
CCNL2	-0.435587918	4.68E-06
CALML4	-0.439427529	5.15E-06
PEMT	-0.439756124	2.88E-07
RCN3	-0.441575774	6.95E-06
SLC22A5	-0.448756838	1.12E-07
ZNF30	-0.449434135	1.10E-05
DYNLL1	-0.450296174	1.67E-09
HDGF	-0.450350765	3.18E-06
OSTC	-0.451671959	3.78E-08
SLC43A1	-0.454547217	6.47E-08

DEPDC7	-0.455420641	3.41E-08
CDK2AP2	-0.455528187	3.84E-05
SUMO3	-0.455542137	3.94E-06
MANF	-0.456365744	2.12E-07
PAICS	-0.458212129	1.48E-06
RGC32	-0.460731887	4.40E-07
GPRC5C	-0.460781042	8.90E-08
RGD1565983	-0.462638247	2.65E-06
PCOLCE	-0.463073432	5.28E-08
CYP2A5	-0.46335112	6.16E-09
PREDICTED:_nucleophosmin-like_[Mus_musculus]	-0.465415093	1.86E-08
HBB	-0.468693565	1.45E-12
EIF3D	-0.478041003	0.0002751
APBB1	-0.478558874	1.97E-05
TRIM24	-0.479056948	1.34E-06
PNPLA8	-0.479617319	1.23E-07
RGD1565772	-0.480185336	1.15E-10

NSUN2	-0.480263904	0.00143
C8A	-0.485146128	0.002092
Human-GAPDH_3	-0.487487896	0.000147
FAM35A	-0.488508585	3.01E-06
ACBD5	-0.488723403	7.87E-06
REEP4	-0.495356107	4.24E-09
SULT2A2	-0.497299666	3.96E-09
ERP29	-0.497989235	7.23E-05
ZFP354B	-0.499114198	1.51E-06
RPL28	-0.499294689	0.005005
TAGLN	-0.501320404	3.84E-08
A1CF	-0.502386648	3.26E-06
PDZK1	-0.502702706	9.84E-10
CRELD2	-0.503952206	2.66E-10
GOLT1A	-0.506499926	0.000195
DMRTA1	-0.507757394	1.86E-06
CD320	-0.508519102	2.33E-06

TECR	-0.509423703	2.42E-05
TREH	-0.512710737	2.69E-10
FAM59A	-0.51438445	5.20E-07
NANP	-0.514838467	9.09E-08
SRP54B	-0.517961325	8.64E-05
LCAT	-0.518526189	0.0003661
SPTBN2	-0.519451643	4.40E-05
HSDL2	-0.521325824	4.47E-11
ECH1	-0.521412353	4.64E-05
KLB	-0.522800267	1.78E-06
PRLR	-0.528003787	3.57E-07
SEC14L2	-0.528547967	3.61E-08
AGPAT3	-0.529356534	6.03E-08
CFH	-0.529848278	9.95E-08
SSR2	-0.530917091	1.18E-09
G6PD	-0.532905638	7.98E-05
GAPDH	-0.535842226	5.22E-06

CADM1	-0.538123162	5.26E-07
UBE2G2	-0.54096137	4.14E-06
CDCA7	-0.544379229	1.97E-05
IGFBP4	-0.544732373	1.11E-05
PTPN9	-0.544785463	1.35E-09
SYS1	-0.544998904	3.72E-05
RPL22L1	-0.546219519	2.40E-08
DDT	-0.54686377	1.64E-08
C21ORF91	-0.548655426	1.51E-05
CISD1	-0.549026761	3.52E-06
SLC37A4	-0.553398608	1.41E-07
ID3	-0.555259743	1.98E-06
ADIPOR2	-0.555368887	1.88E-06
SLC22A21	-0.556888485	2.95E-07
DGKD	-0.557060289	6.11E-08
NME6	-0.558752002	1.18E-07
PDE1C	-0.559521654	1.92E-07

ATF4	-0.559649719	0.001206443
SRP72	-0.560301559	4.49E-06
ALOX5AP	-0.562610953	0.004166072
MAP1LC3A	-0.565839002	0.000333
FAM195A	-0.566248751	6.45E-08
GPRC5A	-0.566249695	1.59E-08
SETDB2	-0.566588192	4.09E-07
ACVR1	-0.568089186	9.30E-07
FTSJ1	-0.571155538	1.37E-08
FMC1	-0.571936531	0.001046
ACAA1	-0.572718822	3.77E-05
RRBP1	-0.574835105	1.64E-05
ZFP54	-0.574843553	0.000568
INSC	-0.575010186	1.71E-05
DYT1	-0.576057211	0.005625813
TDO2	-0.576130623	8.85E-11
1810006K21RIK	-0.576826842	0.001575

C14ORF1	-0.576985196	0.000201
PRDX3	-0.577120151	1.14E-08
SLC16A11	-0.584406522	3.00E-06
PLSCR1	-0.58472416	2.92E-08
SLC10A1	-0.584783495	1.67E-09
CYP4A3	-0.585916026	1.82E-08
RPL36AL	-0.587356378	8.52E-06
PVRL3	-0.587498317	4.04E-11
CYP4A14	-0.589601718	2.89E-10
UGT1A5	-0.592270117	2.99E-10
AMIGO3	-0.592612491	6.45E-07
SRPRB	-0.594872893	0.002912
RNF151	-0.599737484	1.47E-05
SLC43A3	-0.600340054	7.35E-11
DHCR24	-0.600658816	6.09E-09
EBP	-0.603258269	1.46E-05
ACACB	-0.608401384	8.40E-07

RGD1310769	-0.609775881	2.06E-06
CHPF	-0.615279935	3.55E-11
2700060E02RIK	-0.615907325	0.004550773
RNF123	-0.618062409	5.40E-09
LOC360919	-0.620671117	1.02E-05
DIO1	-0.624247815	3.44E-08
C1QA	-0.628889103	8.76E-10
TSPYL2	-0.630667906	2.12E-07
DHRS1	-0.633000472	2.39E-08
FAU	-0.63428024	6.98E-05
DHRS4	-0.636137422	1.96E-05
GMPPA	-0.636627144	6.96E-06
UCK1	-0.641136686	1.41E-05
TLE1	-0.641373077	1.10E-06
HADHA	-0.641425728	2.66E-06
RCL1	-0.642832727	1.01E-12
DDI2	-0.646843303	2.49E-08

DAK	-0.646889119	3.35E-12
TXNL4B	-0.647191559	2.67E-06
LMO2	-0.648812877	3.36E-05
CYP2D40	-0.65163749	9.45E-12
LIPG	-0.656084824	0.000113
RSC1A1	-0.656185363	2.22E-05
ACAA2	-0.659667109	3.62E-08
RPL10	-0.663758468	0.000172
LSS	-0.665860393	1.96E-07
AHSG	-0.666896264	4.76E-05
HDC	-0.667194409	1.77E-09
TM6SF2	-0.669251561	1.09E-06
RGD1304704	-0.66985422	0.00312423
CYP4F1	-0.673580036	0.000232
AVPR1A	-0.677986663	3.19E-09
NSDHL	-0.678293592	4.57E-06
POPDC2	-0.681171492	0.000131

APOA5	-0.681326484	2.23E-06
TMTC2	-0.682858441	4.55E-05
NARS	-0.685054161	4.25E-05
PPAP2B	-0.687078464	3.52E-09
HSP90B1	-0.689357161	9.90E-09
CLDN15	-0.69147533	1.39E-08
MTG1	-0.691855431	2.51E-05
DEPTOR	-0.692288882	0.004513523
CYP2D3	-0.694296112	8.49E-16
CXX1A	-0.698355537	0.0001926
AMBP	-0.698538755	2.99E-08
TMEM66	-0.701720278	2.94E-05
DDOST	-0.702015867	5.65E-06
PDIA4	-0.702592766	5.32E-06
0610007P14RIK	-0.702715037	2.04E-07
ACSM5	-0.703006983	6.64E-05
GJB2	-0.704114394	1.90E-09

ABHD3	-0.705477051	2.94E-11
HBA-A2	-0.706936524	7.26E-11
UPB1	-0.713993883	7.04E-05
F11	-0.715101221	2.68E-11
ACSF2	-0.716212506	1.44E-09
CHCHD2	-0.722776051	7.36E-05
KDELR3	-0.722855334	4.00E-11
HACL1	-0.727886159	1.61E-13
IL33	-0.730360173	3.84E-07
SHMT2	-0.733158338	7.82E-10
CYP8B1	-0.739822593	2.05E-06
RBM14-RBM4	-0.74083857	0.000748
SRM	-0.743058309	0.00032
RBPMS	-0.745269407	6.06E-08
RPL23A	-0.746712173	0.009024687
ATL2	-0.750438154	4.04E-09
CLEC1B	-0.751464723	2.04E-09

ALDH1L1	-0.752155338	2.97E-06
SOCS2	-0.754774093	2.34E-13
FADS1	-0.758938541	6.06E-11
MAGED1	-0.760481517	7.97E-05
FKBP5	-0.76329088	2.66E-10
BMP1	-0.775213151	5.19E-11
LRRC3	-0.782501886	3.37E-08
STMN2	-0.796219794	7.89E-09
AMY2B	-0.801503877	6.84E-09
SERPINA5	-0.802380201	9.80E-14
C1GALT1C1	-0.805134519	0.0001472
Dhdh_protein_[Mus_musculus]	-0.805857801	4.05E-12
INHBA	-0.807198956	5.16E-11
TSPAN31	-0.813271481	3.63E-05
RALGPS2	-0.823214927	0.000216
SLC26A6	-0.832033	5.33E-14
CRAT	-0.832471603	3.05E-08

ALDH8A1	-0.838935927	4.02E-05
STIP1	-0.851428912	8.82E-05
FASN	-0.858451581	2.31E-09
MORF4L2	-0.863404529	0.008172
5730455O13RIK	-0.880469027	3.19E-05
PANK1	-0.884306755	6.15E-06
ATF5	-0.886714006	1.19E-07
UGT2B1	-0.888111469	7.70E-11
HES6	-0.893895442	1.28E-07
SRD5A1	-0.895519202	3.31E-06
MSMB	-0.89854709	4.20E-11
HSPA5	-0.900055356	2.30E-08
PCSK6	-0.902328378	7.21E-08
COPB2	-0.904342111	0.004104
SLPI	-0.904751228	3.31E-12
ACSS3	-0.90481259	3.36E-06
RDH11	-0.906251349	2.70E-08

AGMAT	-0.908518945	1.37E-11
SLC25A15	-0.91297987	3.80E-05
FGF21	-0.91586438	2.00E-08
TXNIP	-0.920775229	1.84E-05
RETSAT	-0.922105921	4.19E-08
ERRFI1	-0.927572859	5.05E-05
PDK4	-0.927917301	1.19E-06
ACOX1	-0.932444144	1.55E-08
SSR4	-0.933130267	8.98E-06
EHHADH	-0.943428981	3.09E-11
REEP6	-0.95137491	8.35E-13
TPD52L1	-0.953883396	1.28E-09
SNTB1	-0.956007991	2.35E-08
ARF4	-0.959930076	0.001221779
DBI	-0.966119812	3.82E-10
SYT9	-0.966598796	4.52E-11
LEF1	-0.972358935	1.11E-08

RASD1	-0.974559945	3.66E-11
HN1L	-0.986503261	2.46E-06
G6PC	-0.987233353	1.16E-13
IGJ	-0.990505625	1.37E-05
B_Chain_B._Structure_Of_Jmjd6_And_Fab_Fragments	-0.992553966	3.78E-09
FKBP11	-0.995724275	3.03E-15
ACSL1	-1.011095456	1.78E-09
TAF1D	-1.011715704	0.000309
PLIN2	-1.014935162	1.84E-07
IGFBP1	-1.019558221	1.15E-16
ADH6	-1.020606691	2.62E-07
CYP2D34	-1.021848788	6.12E-17
PACAP	-1.021860337	6.18E-07
DND1	-1.025058357	1.29E-06
SDPR	-1.025796607	5.85E-06
ACLY	-1.03525386	2.62E-06
MUG2	-1.044257409	2.64E-12

SC5DL	-1.059012984	4.98E-06
ITM2A	-1.087829311	0.000118
PPM1K	-1.102814756	5.00E-04
PGLYRP2	-1.103314003	1.17E-16
HMGCR	-1.114748093	2.55E-11
ACSL5	-1.120176972	1.62E-05
SLC17A1	-1.141680301	6.30E-10
TMEM45B	-1.157961033	3.40E-07
FDPS	-1.163057002	2.86E-15
CYP2F4	-1.172062106	4.36E-06
ANGPTL4	-1.18517893	1.99E-14
FGB	-1.185615488	7.28E-06
ASS1	-1.191082027	1.03E-06
HSD17B12	-1.198362319	5.20E-05
ARG1	-1.219729137	0.0001108
ECI2	-1.234107703	6.42E-10
EGR1	-1.270857058	0.0001766

RAB30	-1.27733842	7.23E-08
RGD1564575	-1.28403 6415	9.35E-13
FOS	-1.28600 973	4.56E-18
FGL1	-1.30948 526	1.35E-15
PEG3	-1.31506 2411	4.80E-06
INSIG1	-1.39050 5193	5.92E-15
CTSF	-1.39645 9282	7.50E-15
ACMSD	-1.43399 0891	4.46E-06
PCK1	-1.45707 5138	9.97E-16
LECT2	-1.47565 4752	6.38E-08
MUG1	-1.48063 4062	5.94E-15
AK4	-1.50387 6981	1.94E-10
A2M	-1.50490 5321	1.02E-16
SERPINF1	-1.51032 0203	2.28E-16
SAA3	-1.51848 6997	1.13E-20
A1I3	-1.56165 9939	5.28E-13
ANKRD29	-1.56356 0959	4.10E-11

CXCL13	-1.568885784	3.06E-05
MFSD2	-1.582812594	2.68E-08
TMEM97	-1.614086795	8.81E-05
SLC5A8	-1.703004338	2.87E-08
CD163	-1.707789928	1.67E-09
PSAT1	-1.716152094	8.58E-11
DHCR7	-1.721930011	0.001496585
SLC25A47	-1.727114818	6.96E-11
HMGCS1	-1.780157221	6.78E-13
LPIN1	-1.789525415	2.18E-10
IDI1	-1.814298636	1.32E-08
STARD4	-1.841022454	5.20E-07
CYP4B1	-2.064659943	7.11E-12
LCN14	-2.121080576	9.84E-14
FDFT1	-2.181899585	1.63E-17
SQLE	-2.957134703	5.26E-07

Supplementary table 4. Metabolites identified by NMR. The mean Logarithm of the HFD to STD foldchange is represented together with the SEM, the p-value of the Staudent's T contrast and the q-value of the False discovery rate (FDR) calculated by the Benjamini-Hotchberg method.

	Log FC	SEM	p-value	FDR
Cholesterol				
Oleic Acid cholesterol Esters	3.464	0.059	1.3E-08	5.2E-07
Esterified Cholesterol	7.219	0.086	9.4E-08	1.8E-06
Free Cholesterol	2.250	0.069	1.8E-07	2.8E-06
Total Cholesterol	5.334	0.076	5.3E-08	1.4E-06
Glycerolipids				
Serine	0.142	0.083	3.7E-01	4.5E-01
Free glycerol	0.097	0.165	6.2E-01	7.1E-01
Myo-inositol	-0.361	0.064	5.1E-03	2.2E-02
O-PhosphoCholine	-0.661	0.105	2.7E-02	5.3E-02
Ethanolamine	-0.432	0.099	6.2E-03	2.2E-02
sn-Glycero phosphocholine	0.517	0.035	3.0E-03	1.5E-02
Plasmalogen	0.490	0.025	2.6E-03	1.5E-02
Lysophosphatidyl choline	0.513	0.023	5.7E-06	7.3E-05
Sphingomyelin	0.243	0.019	3.5E-02	6.4E-02
Phosphatidylinositol	-0.025	0.083	9.2E-01	9.3E-01

Phosphatidylethanolamine	-0.340	0.043	6.0E-03	2.2E-02
Phosphatidylcholine	-0.216	0.022	1.7E-02	4.1E-02
Total Phospholipids	-0.263	0.027	5.1E-03	2.2E-02
Diglycerides	0.453	0.048	1.9E-03	1.2E-02
Triglycerides	-0.149	0.046	3.5E-01	4.4E-01
Fatty acids metabolism				
Acetate	-0.637	0.247	1.1E-01	1.7E-01
3-hydroxy butyrate	-0.237	0.154	4.2E-01	5.1E-01
Omega-3	-0.013	0.017	9.2E-01	9.3E-01
arachidonic+Eicosapentaenoic acids	-0.380	0.026	1.0E-02	2.8E-02
oleic acid	3.464	0.059	1.3E-08	5.2E-07
Docosahexaenoic acid	-0.012	0.035	9.1E-01	9.3E-01
polyunsaturated fatty acids	-0.054	0.024	6.3E-01	7.1E-01
Energy and Red-Ox status				
Glutathione (ox)	-0.528	0.092	7.2E-03	2.2E-02
Creatine	-0.350	0.084	6.8E-03	2.2E-02
Nicotinamide Mononucleotide (NMN)	-1.919	0.126	2.4E-02	4.8E-02
NADP+	-0.847	0.235	3.4E-02	6.3E-02
NAD+	-0.356	0.221	3.1E-01	4.0E-01

NADH	-0.802	0.082	1.2E-02	3.2E-02
GTP	-0.574	0.144	1.9E-02	4.3E-02
AMP	-0.635	0.136	6.6E-03	2.2E-02
ADP	-1.442	0.292	2.2E-02	4.6E-02
ATP	-0.085	0.137	8.4E-01	8.9E-01
Aminoacids and one carbon metabolism				
Formate	-0.587	0.088	2.6E-04	2.9E-03
Methionine	-0.697	0.104	3.0E-03	1.5E-02
Glutathione (ox)	-0.528	0.092	7.2E-03	2.2E-02
Choline	-0.700	0.130	4.6E-02	7.6E-02
Taurine	0.050	0.220	3.6E-01	5.5E-01
Lysine	-0.367	0.100	1.7E-02	4.1E-02
Glycine	-0.266	0.074	1.4E-01	2.0E-01
Betaine	0.241	0.122	2.5E-01	3.4E-01
Serine	0.142	0.083	3.7E-01	4.5E-01
Carnosine	-0.637	0.138	8.4E-03	2.5E-02
Aspartate	-0.966	0.198	9.4E-03	2.7E-02
Asparagine	-0.595	0.095	1.3E-02	3.3E-02

Histidine	-0.328	0.095	3.6E-02	6.4E-02
Inosine	-0.452	0.072	6.5E-02	1.0E-01
Glutamine	0.347	0.092	1.0E-01	1.6E-01
Glutamate	-0.534	0.122	1.4E-01	2.0E-01
Ornithine	-0.199	0.081	2.8E-01	3.7E-01
Isoleucine	-0.134	0.064	4.8E-01	5.7E-01
Alanine	-0.219	0.148	5.1E-01	6.0E-01
Trypthophan	0.074	0.170	6.9E-01	7.7E-01
Valine	0.034	0.072	7.5E-01	8.2E-01
Phenylalanine	-0.078	0.104	7.5E-01	8.2E-01
Leucine	0.032	0.070	7.8E-01	8.4E-01
Tyrosine	-0.012	0.065	9.7E-01	9.7E-01
beta-Alanine	-0.234	0.078	1.6E-01	2.2E-01
carbohydrate metabolism				
Uracil	-0.189	0.093	3.4E-01	4.3E-01
Guanosine*	-0.623	0.168	3.7E-02	6.4E-02
Uridine	-0.736	0.100	3.3E-02	6.3E-02
Glycogen	1.870	0.240	2.0E-02	4.3E-02
Lactate	0.335	0.153	1.9E-01	2.6E-01

UDP-Glucuronate	-0.348	0.107	1.3E-01	1.9E-01
UDPGs	-0.344	0.070	4.3E-02	7.3E-02
Glucose	1.014	0.212	2.0E-02	4.3E-02
UDP-NAcGlu	-0.576	0.090	3.4E-03	1.6E-02
UDP-2AcGlu	-0.818	0.161	1.4E-03	1.0E-02

Supplementary table 4. Go terms and gene set enrichement analysis associated to the network presented in figure 5a. Results were obtained with the Genemania plugin for Cytoscape 3.

GO id	Description	q-value	Occurrences in Sample	Occurrences in Genome
GO:0000785	chromatin	9.80E-09	10	212
GO:0044212	transcription regulatory region DNA binding	2.44E-08	10	266
GO:0001067	regulatory region nucleic acid binding	2.44E-08	10	267
GO:0000975	regulatory region DNA binding	2.44E-08	10	267
GO:0000775	chromosome, centromeric region	3.03E-05	6	98
GO:0001085	RNA polymerase II transcription factor binding	3.06E-04	5	74
GO:0032993	protein-DNA complex	3.31E-04	6	158
GO:0007062	sister chromatid cohesion	3.31E-04	4	30
GO:0001102	RNA polymerase II activating transcription factor binding	3.54E-04	4	32
GO:0008278	cohesin complex	7.77E-04	3	10
GO:0006352	DNA-templated transcription, initiation	0.001361066	6	212
GO:0033613	activating transcription factor binding	0.001410646	4	48
GO:0000790	nuclear chromatin	0.002277874	5	131
GO:0000228	nuclear chromosome	0.002277874	6	239
GO:0043425	bHLH transcription factor binding	0.003495051	3	18
GO:0003705	RNA polymerase II distal enhancer sequence-specific DNA binding transcription factor activity	0.003843497	4	66

GO:0090329	regulation of DNA-dependent DNA replication	0.007601244	3	24
GO:0043392	negative regulation of DNA binding	0.008149354	3	25
GO:0000793	condensed chromosome	0.009131253	4	86
GO:0006367	transcription initiation from RNA polymerase II promoter	0.009131253	5	189
GO:0070888	E-box binding	0.009131253	3	27
GO:0033044	regulation of chromosome organization	0.009657242	4	90
GO:0000981	sequence-specific DNA binding RNA polymerase II transcription factor activity	0.010701714	5	199
GO:0008156	negative regulation of DNA replication	0.010732646	3	30
GO:0044454	nuclear chromosome part	0.012475811	5	209
GO:0044786	cell cycle DNA replication	0.015887399	3	35
GO:0003713	transcription coactivator activity	0.026760533	5	249
GO:0007059	chromosome segregation	0.030409045	4	128
GO:0051101	regulation of DNA binding	0.032657678	3	46
GO:0003682	chromatin binding	0.048669799	4	147
GO:0007179	transforming growth factor beta receptor signaling pathway	0.050941525	4	150

GO:0051053	negative regulation of DNA metabolic process	0.053481828	3	56
GO:0003714	transcription corepressor activity	0.064462785	4	162
GO:0051100	negative regulation of binding	0.065011796	3	61
GO:0000791	euchromatin	0.067687779	2	11
GO:0071560	cellular response to transforming growth factor beta stimulus	0.067687779	4	169
GO:0071559	response to transforming growth factor beta	0.067687779	4	169
GO:0051052	regulation of DNA metabolic process	0.084000659	4	180

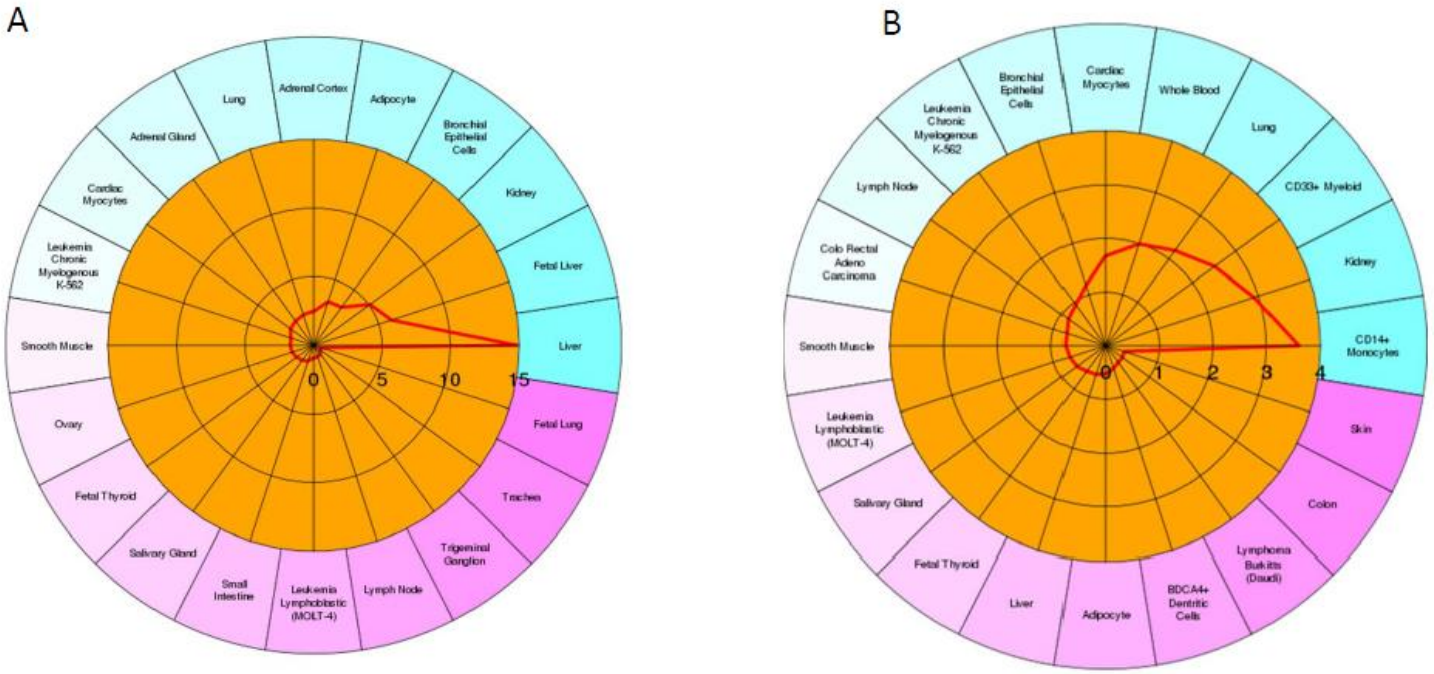

Supplementary figure 1. Tissue type profiling using the differencially changed genes of the microarray analyses in the CTEN software. All changed genes (A) or only the upregulated genes (B)were analysed. Figures are the output of the software and show the score obtained for each tissue (red line).

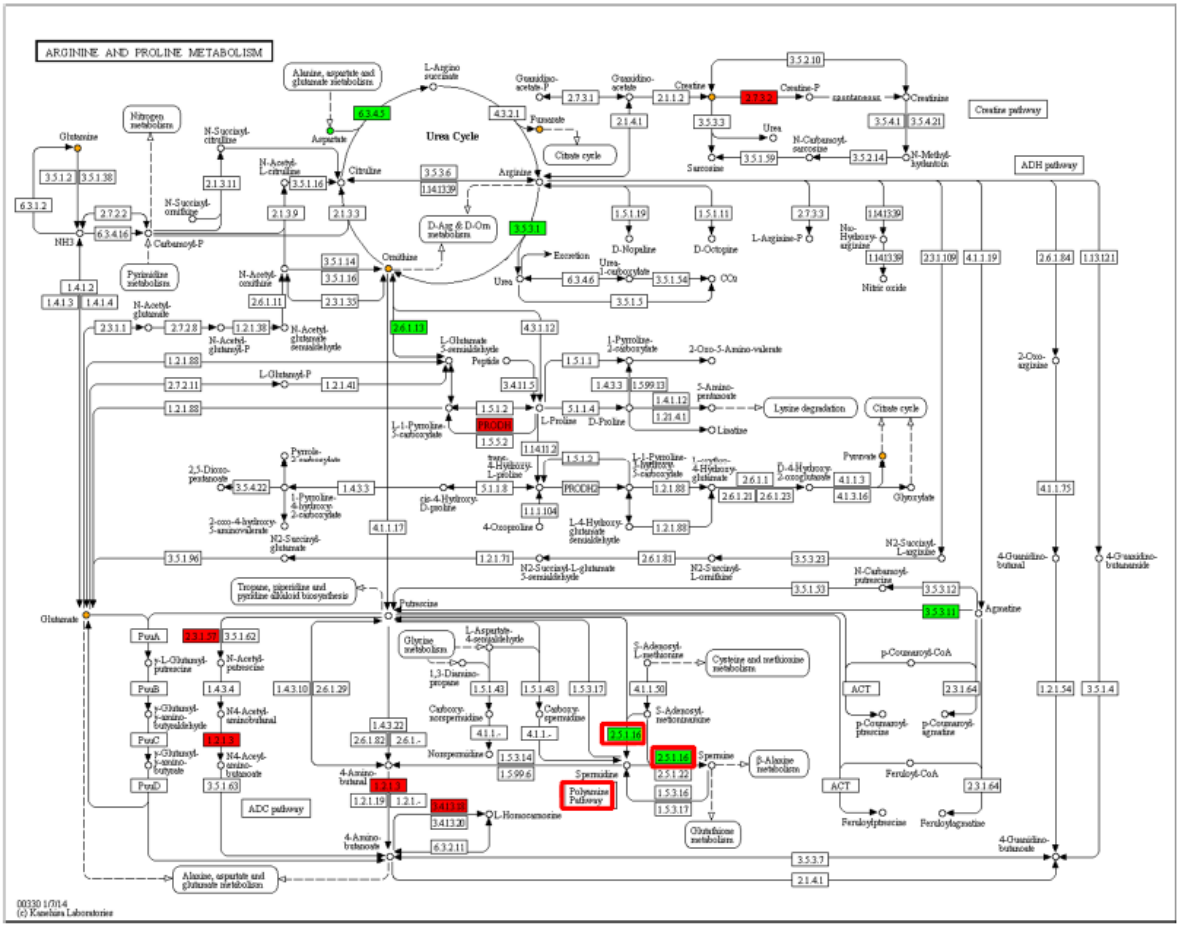

Supplementary figure 2. Kegg pathway map00330, Arginine and proline metabolism. Differentially expressed genes (Squares; green, downregulated; red upregulated in HFD respect STD group) and metabolites (Circles; white, not determined; orange, not changed; green, decreased; red, increased in HFD respect STD group) were implemented in KEGG maps using the KEGG mapper (http://www.kegg.jp/kegg/tool/map_pathway2.html). Polyamine pathway and spermidine synthase (*SRM*) have been highlighted in red.

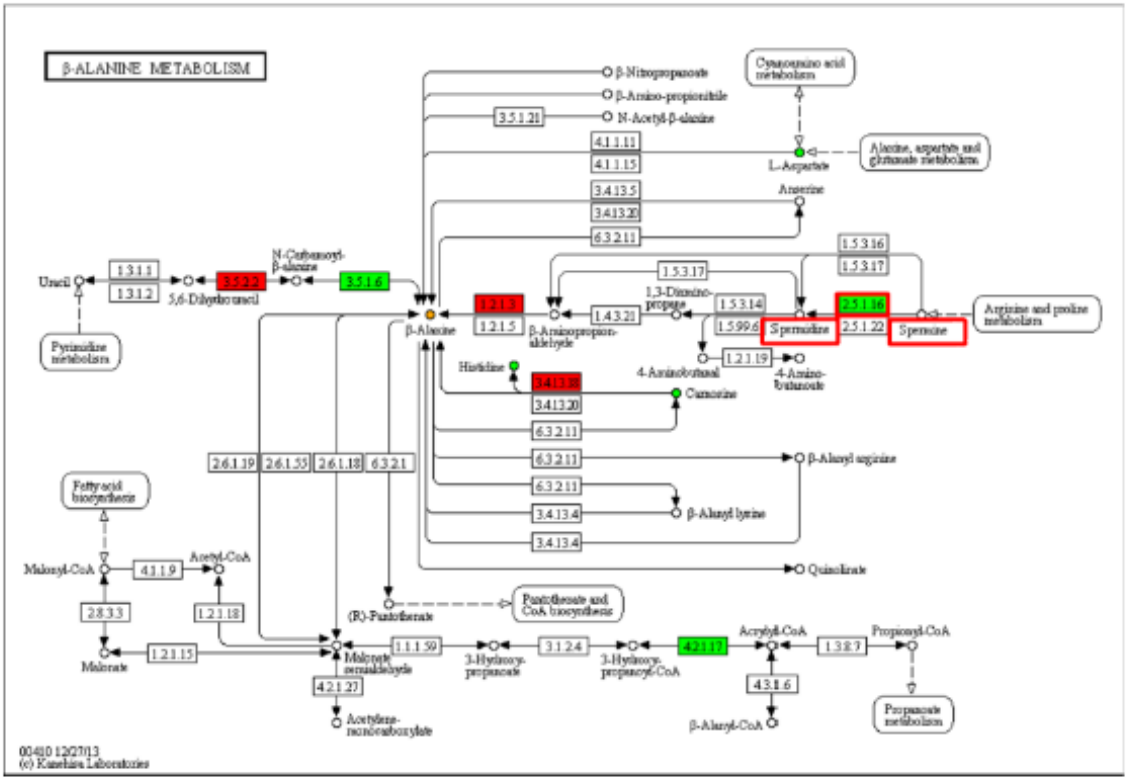

Supplementary figure 3. Kegg pathway map00410, β-Alanine metabolism. Differentially expressed genes (Squares; green, downregulated; red upregulated in HFD respect STD group) and metabolites (Circles; white, not determined; orange, not changed; green, decreased; red, increased in HFD respect STD group)) were implemented in KEGG maps using the KEGG mapper (http://www.kegg.jp/kegg/tool/map_pathway2.html). Spermidine, spermine and spermidine synthase (*SRM*) have been highlighted in red.

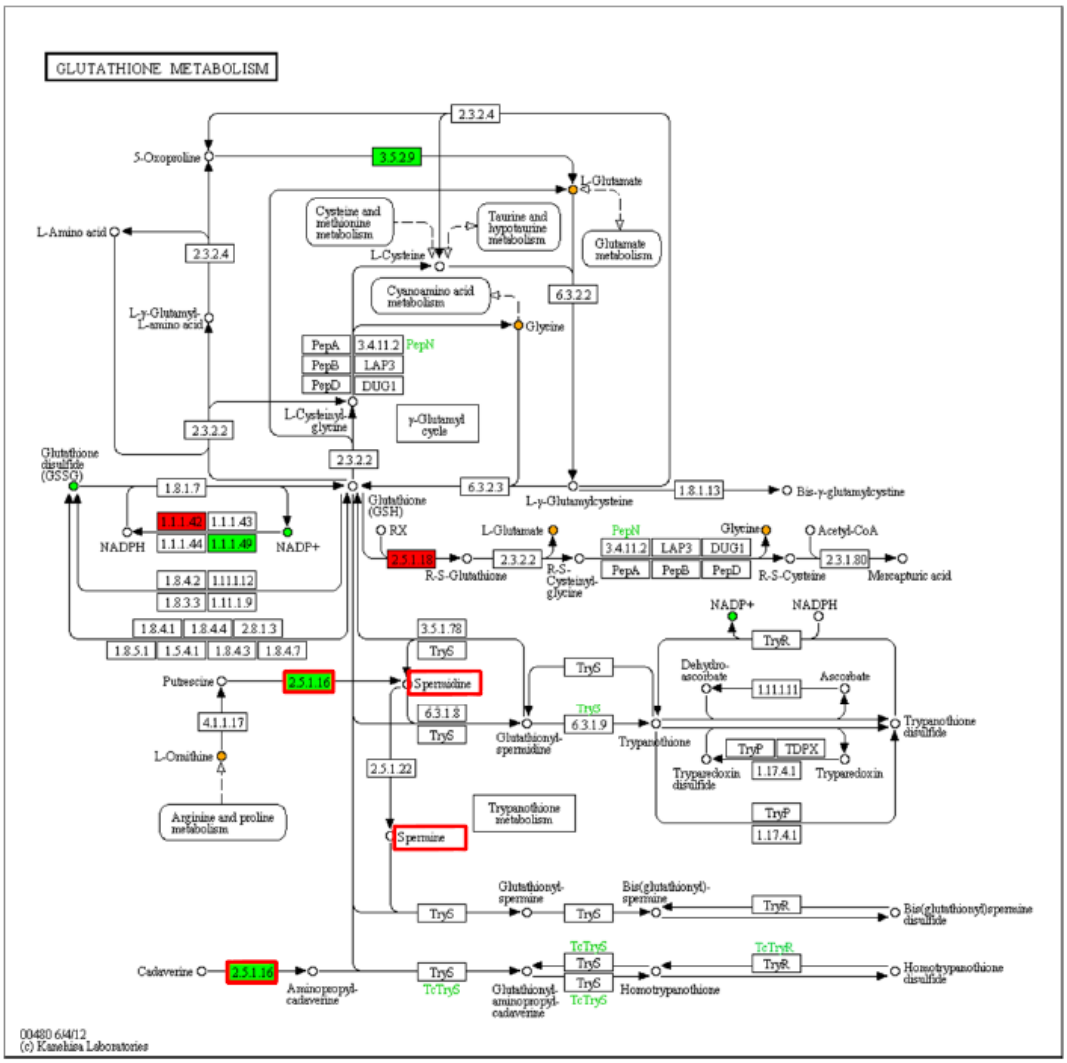

Supplementary figure 4. Kegg pathway map00480, Glutathione metabolism. Differentially expressed genes (Squares; green, downregulated; red upregulated in HFD respect STD group) and metabolites (Circles; white, not determined; orange, not changed; green, decreased; red, increased in HFD respect STD group) were implemented in KEGG maps using the KEGG mapper (http://www.kegg.jp/kegg/tool/map_pathway2.html). Spermidine, spermine and spermidine synthase (*SRM*) have been highlighted in red.

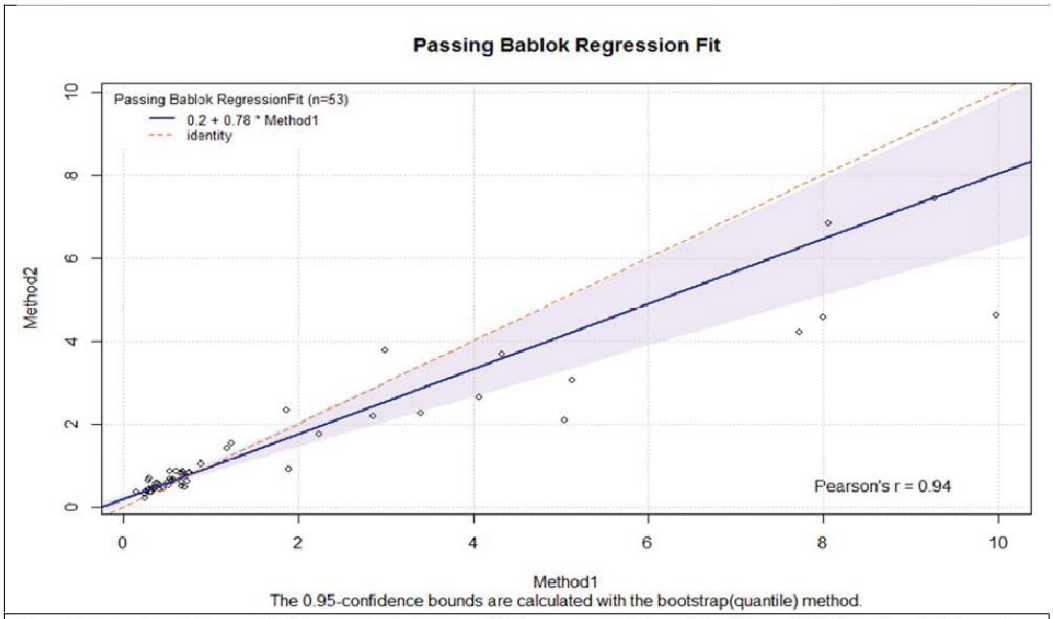

Supplementary figure 5. The fold change of 53 genes obtained by RT-q-PCR (method 1) and hamster microarray (method 2) were used for Passing and Bablok regression fit .